NASA
Technical
Paper
2474

May 1985

A Critical Evaluation of Various Turbulence Models as Applied to Internal Fluid Flows

M. Nallasamy

NASA

NASA Technical Paper 2474

1985

A Critical Evaluation of Various Turbulence Models as Applied to Internal Fluid Flows

M. Nallasamy

George C. Marshall Space Flight Center
Marshall Space Flight Center, Alabama

NASA
National Aeronautics and Space Administration

Scientific and Technical Information Branch

ACKNOWLEDGMENTS

The author expresses his thanks to Dr. C. P. Chen, National Research Council Fellow at Marshall Space Flight Center, Fluid Dynamics Branch, for many helpful discussions during the preparation of this report. The author is grateful to Dr. G. Fichtl, Dr. N. C. Costes and Dr. W. Campbell for reviewing the manuscript and for many helpful comments.

This work was supported by USRA contract NAS8-35918, SSME Internal Flow Processes.

TABLE OF CONTENTS

NOMENCLATURE

C	coefficients in turbulence models
c_f	friction coefficient
d, D	diameter or width of the channel
E	friction factor in law of the wall
$\overline{f}$, f'	mean and fluctuating components of variable f
G	buoyancy production/destruction of $k = -\beta\, g_i\, \overline{u_i \phi}$
G_{ij}	buoyancy production/destruction of $\overline{u_i u_j} = -\beta\, (g_i u_j\, \phi + g_j u_i\, \phi)$
g	gravitational acceleration
H	step height
k	turbulence kinetic energy, $1/2\ \overline{u_i u_j}$
l_m	mixing length
l	turbulence length scale
Nu	Nusselt number
p	pressure
Pe	Peclet number
R_{ij}	Reynolds stress
Re	Reynolds number
R_c	mean radius of curvature
R_t	turbulence Reynolds number
R_i	gradient Richardson number
R_f	flux Richardson number
R_{ic}	curvature Richardson number
S	swirl number
U, V, W	mean velocity in x, y, z directions
u, v, w	fluctuating velocities in x, y, z directions
U_i	mean velocity component in x_i direction
u_i	fluctuating velocity components in x_i direction

U_τ	friction velocity
x,y,z	Cartesian coordinates
x_i	coordinate in tensor notation
X_R	reattachment length
y^+	dimensional distance, $y\ U_\tau/\nu$
β	volumetric expansion coefficient
Γ	circulation, equation (53)
Γ_f	false diffusion
δ_{ij}	Kronecker delta
ϵ	dissipation rate of turbulence energy
η	subgrid scale Reynolds stress
θ	polar coordinate
κ	von Karman constant
μ	dynamic viscosity
μ_{eff}	effective dynamic viscosity ($\mu + \mu_t$)
ν	kinematic viscosity
ν_t	turbulence kinematic viscosity
ρ	fluid density
σ_k, σ_ϵ	turbulent Prandtl number for diffusion of k and ϵ
τ	turbulence shear stress
τ_w	wall shear stress
ϕ	fluctuating scalar quantity
ψ	stream function
ω	vorticity (eqs. 53, 55, and 56), time-mean square vorticity fluctuations (eqs. 7 and 10)

TECHNICAL PAPER

A CRITICAL EVALUATION OF VARIOUS TURBULENCE MODELS AS APPLIED TO INTERNAL FLUID FLOWS

I. INTRODUCTION

Turbulence is one of the unsolved problems in the area of physical sciences. It is believed that the solution of time-dependent three-dimensional Navier-Stokes equations can describe turbulent flows completely. However, the computers are not large and fast enough to solve the equations directly, for the required range of length and time scales, even for simple flows. Many industrially important flows, such as the flow in a space shuttle main engine, are quite complex. Hence, it is of practical importance to describe turbulent motion in terms of time averaged quantities rather than instantaneous. This kind of description leads to the well known turbulence closure problem [1]. Substitution of apparent mean (Reynolds) stresses for the actual transfer of momentum by the velocity fluctuations increases the number of unknowns above the number of equations. The problem is then to supply the information missing from the time-averaged equations by formulating a model to describe some or all of the six independent Reynolds stresses, $-\rho\ \overline{u_i u_j}$. The exact Reynolds stress transport equations can be derived from the time-dependent Navier-Stokes equations [2]. These equations express the conservation of each Reynolds stress as the Navier-Stokes equations express the conservation of each component of momentum. In turbulence modeling one uses a finite number of Reynolds stress transport equations with the supply of missing information from experimental results. The time-averaged scalar transport equation contains the turbulent heat or mass flux, $-\rho\ \overline{u_i \phi}$, where ϕ is the fluctuating scalar quantity. One has to model this term to solve the scalar transport equation.

First order closure or mean velocity field closure expresses the Reynolds stresses as a function of the mean velocity field. Closure of the Reynolds stress transport equations requires third-order mean products of velocity fluctuations to be expressed in terms of second-order mean products (the Reynolds stresses themselves) and is known as second order closure or Reynolds stress closure.

First, this report describes the equations of turbulent flow, and then the turbulence models which are often used in engineering calculations. Then it discusses the application of the models and their performance in internal flows which are of particular interest here. Internal flow encompasses a wide range of flows and can be extremely complex. It includes fluid flow in pipes, passages, ducts, conduits, and in components such as bends, diffusers, and heat exchangers. Like a majority of all turbulence researches, the report deals with incompressible flows.

II. EQUATIONS OF MOTION

If the flow variables are assumed to be of the form $f = \overline{f} + f'$ where $\overline{f}$ is the mean value of f and f' is the fluctuation about the mean, one can obtain the time averaged continuity and momentum equations [2,3]

$$\frac{\partial \overline{u_i}}{\partial x_i} = 0 \qquad (1)$$

$$\frac{\partial \bar{u}_i}{\partial t} + \bar{u}_j \frac{\partial \bar{u}_i}{\partial x_j} = -\frac{1}{\rho}\frac{\partial \bar{p}}{\partial x_i} + \frac{\mu}{\rho}\nabla^2 \bar{u}_i - \frac{\partial R_{ij}}{\partial x_j} \tag{2}$$

where $R_{ij} = \overline{u_i u_j}$, the Reynolds stress. In order to establish a turbulence model that is less complicated than the full equations, it is necessary to establish a way of evaluating R_{ij} in terms of the variable $\bar{u}_i$, higher-order turbulence statistics and some constants evaluated from experimental data. The various turbulence models employed for the closure of the mean equations are discussed next.

III. TURBULENCE MODELS

The numerical procedures which are associated with turbulence models to make complete calculation methods can be divided into integral and differential types. Differential methods involve direct assumptions for the Reynolds stresses at a point and seek the solution of the governing equation in their partial differential equation form.

Integral methods involve the integral parameters of the shear layer momentum thickness, shape parameter, skin friction coefficient, etc. One solves a system of ordinary differential equations (for two-dimensional flows), whose dependent variables are the profile parameters and independent variable is x; in three-dimensional flows, the equations are the partial differential equations in the plane of the layer. The important distinction between calculation methods is the type of turbulence model rather than the type of numerical procedure.

The advantage of differential methods is that the restrictions and inaccuracy that arise from the need to parameterize the velocity profiles are avoided. Differential methods introduce substantially more detailed information about turbulence. Here modeled forms of governing equations and the corresponding closures for the differential methods are described.

The turbulence models can be classified in several ways. The one most often used is that arranged in order of the number of differential equations solved in addition to the mean flow equations [4]

(I) Zero equation models

(II) One equation models

(III) Two equation models

(IV) Stress equation models

Most of the models, classes (I) to (III), use Boussinesq eddy viscosity model. Bradshaw, et al. [5], however, assume the constancy of the $\tau/\rho k$ ratio, in boundary layer flows. Here τ is the shear stress and k is the turbulent kinetic energy. It is important to note here that in this case the mean momentum and continuity equations form a hyperbolic system in contrast to the parabolic system obtained with the use of eddy viscosity models [6]. Other models which do not use the eddy viscosity assumption (class IV) obtain the Reynolds stress from a differential equation.

Zero equation model, which uses only the partial differential equation for the mean flow field and no transport equations for turbulence quantities, is also called "mean field" closure [7]. The classes (II) to (IV) are called "transport equation" closures. Yet another classification is based on the highest order of velocity product for which a transport equation is used. Zero equation models use partial differential equations for the U_i only and are therefore "first order" models. Classes (II) to (IV) use partial differential equations for $\overline{u_i u_j}$ and are "second order" closures, while some class (IV) models use transport equation for third order products $\overline{u_i u_j u_l}$ [4].

Bradshaw [8] describes the interplay between the development of models and the experiments. The monograph by Launder and Spalding [9] gives the mathematical concepts of turbulence models. Bradshaw and Cebeci [10] describe the calculation methods for various classes of turbulent flows. Gosman, et al. [11] present various aspects of computation of recirculating flows. They form the basis of many of the current turbulent flow computational schemes. Several reviews have appeared recently concentrating on specific aspects of turbulence modeling [12 to 21]. This report concentrates on the turbulence models and their applications to internal flows. In the following, the main classes of turbulence models are described briefly.

3.1. Zero Equation Models

Zero equation models are mostly based on the eddy viscosity concept. This concept stems from the convenience associated with maintaining an approach, for turbulent flows, which is similar to that for laminar flows. This convenience of concept is coupled with the possible mathematical convenience of retaining the same form of differential equations for laminar and turbulent flows and allowing the use of the same solution procedure.

The first turbulence model proposed, the Prandtl's mixing length hypothesis, is still among the most widely used models. It employs the eddy viscosity concept which relates the turbulent transport terms to the local gradient of mean flow quantities. For example, for thin shear layers

$$- \overline{uv} = \nu_t \frac{\partial U}{\partial y} \tag{3}$$

where

ν_t = eddy viscosity.

The Prandtl mixing length hypothesis calculates the distribution of eddy viscosity by relating it to the mean velocity gradient

$$\nu_t = C_\mu \, l_m^2 \left| \frac{\partial U}{\partial y} \right| \tag{4}$$

This relation involves a single unknown parameter, the mixing length l_m whose distribution over the flow field has to be prescribed with the aid of empirical information. C_μ is a constant. The mixing length model has been used for thin shear layers and wall boundary layers [16]. The main drawback with this model is the evaluation of l_m for different flows. The evaluation of l_m becomes difficult for recirculating flows and three-dimensional flows. In the already empirical specification of the mixing length, it is difficult to incorporate in any useful manner, the effects of curvature, buoyancy or rotation. The transport and history effects of turbulence are not accounted in the mixing length model. The more generally applicable models to be described below account for these effects by introducing transport equations for turbulent quantities.

3.2. One Equation Models

The one equation model requires the solution of an equation for the turbulent kinetic energy, k, and, as a result, allows for its transport. The turbulent kinetic energy equation can be derived from the Navier-Stokes equations [12]. The eddy viscosity is modeled by $\nu_t = C_\mu\, k^{1/2}\, l$. The length scale l is specified algebraically and hence is flow dependent. This approach is not very popular since it performs only marginally better than the zero equation model.

3.3. Two Equation Models

This class of models is the one widely used in present day engineering calculations. In attempts to eliminate the need for specifying the turbulence length scale as a function of position throughout the flow, a second differential equation which in effect gives l has been used.

In general, one looks for an equation for a quantity that is a combination of k and l, $Z = k^\alpha\, l^\beta$. Such an equation can also be derived from the Navier-Stokes equations. It has the form [12,22],

$$\rho \frac{DZ}{Dt} = \frac{\partial}{\partial y}\left(\frac{\mu_t}{\sigma_Z}\frac{\partial Z}{\partial y}\right) + Z\left[C_1 \frac{\mu_t}{k}\left(\frac{\partial U}{\partial y}\right)^2 - C_2\, \rho^2 \frac{k}{\mu_t}\right] + S_Z \quad . \tag{5}$$

Here σ_Z is a Prandtl number for the diffusion of Z, S_Z is a secondary source term which appears in some models, and C_1 and C_2 are constants.

The Imperial College group lead by Prof. Spalding has experimented with three different kinds of two equation models [21]: k–kl; k–ω, and k–ϵ. l is a length representing the macroscale of turbulence which may be defined in terms of k, ϵ and a constant C_D through

$$l = C_D\, k^{3/2}/\epsilon \tag{6}$$

ω is a quantity having the dimensions of $(\text{time})^{-2}$ which has been interpreted as representing the time average square of the vorticity fluctuations, and it can also be defined in terms of k, ϵ and C_D.

$$\omega = \epsilon^2/(C_D k)^2 \tag{7}$$

and ϵ is defined by

$$\epsilon = \nu \overline{\frac{\partial u_i}{\partial x_k} \frac{\partial u_i}{\partial x_k}} \tag{8}$$

The above definitions imply that

$$\frac{dkl}{kl} = 5/2 \frac{dk}{k} - \frac{d\epsilon}{\epsilon} \tag{9}$$

$$\frac{d\omega}{\omega} = -2 \frac{dk}{k} + 2 \frac{d\epsilon}{\epsilon} \quad . \tag{10}$$

With the aid of these equations, it is possible to transform one pair of equations into another [21]. Thus, the three models differ only in the mathematical form but not in content. However, the k-ϵ model has become most popular because of the practical advantage that the ϵ-equation requires no extra terms near walls. Also, ϵ itself appears in the k-equation and the ϵ equation requires no secondary source term. Hence, only the k-ϵ model is described in detail here.

The k-ϵ model employs the eddy viscosity and relates the eddy viscosity to k and ϵ. One solves two differential equations, one for turbulent kinetic energy and the other for its dissipation. The modeled equations for k and ϵ are given below [21]:

(a) Kinetic energy equation:

$$\frac{Dk}{Dt} = \frac{1}{\rho} \frac{\partial}{\partial x_k} \left[\frac{\mu_t}{\sigma_k} \frac{\partial k}{\partial x_k} \right] + \frac{\mu_t}{\rho} \left(\frac{\partial U_i}{\partial x_k} + \frac{\partial U_k}{\partial x_i} \right) \frac{\partial U_i}{\partial x_k} - \epsilon \quad . \tag{11}$$

(b) Kinetic energy dissipation rate equation:

$$\frac{D\epsilon}{Dt} = \frac{1}{\rho} \frac{\partial}{\partial x_k} \left[\frac{\mu_t}{\sigma} \frac{\partial \epsilon}{\partial x_k} \right] + \frac{C_1 \mu_t}{\rho} \frac{\epsilon}{k} \left(\frac{\partial U_i}{\partial x_k} + \frac{\partial U_k}{\partial x_i} \right) \frac{\partial U_i}{\partial x_k} - C_2 \frac{\epsilon^2}{k} \tag{12}$$

$$\mu_t = C_\mu \rho k^2/\epsilon \quad . \tag{13}$$

The constants in these equations have been found to take the following values [21].

$C_\mu = 0.09$

$C_1 = 1.44$

$C_2 = 1.92$

$\sigma_k = 1.0$

$\sigma_\epsilon = 1.3.$

The coefficients are constants in the sense that they are not changed in any calculation. However, these constants need to be changed in order to accommodate the effects such as curvature, low Reynolds number, near wall, etc.

Close to the walls, the local Reynolds number of turbulence is small and the molecular transport becomes important. To resolve the wall layer properly in a numerical solution procedure one requires an extremely fine mesh near the wall. Fine mesh size increases the computational time by an order of magnitude. Hence, most computational schemes avoid it by using the wall function to bridge the whole of the wall layer to the fully turbulent region. The first computational point p near the wall (Fig. 1) is to be located in the fully turbulent log-law region. The momentum flux at such a point p satisfies the relation [21]

$$\frac{U_p}{(\tau/\rho)_w} C_\mu^{1/4} k_p^{1/2} = \frac{1}{\kappa} \ln \left[E y_p \frac{(C_\mu^{1/2} k_p)^{1/2}}{\nu} \right] . \tag{14}$$

Here U_p is the velocity of the fluid at the point p along the wall and τ_w is the shear stress at the wall in the direction of U_p. The quantity k_p, the value of k at the grid point P, is computed by assuming that the generation and dissipation of energy are equal in the wall layer where the shear stress is uniform and the length scale is proportional to the distance from the wall. The quantity E is a function of wall roughness and is equal to 9 for smooth walls. Extensive accounts of wall functions and their manner of application are discussed in References 11 and 21. Recent formulations of near-wall treatments are discussed in Section IV.

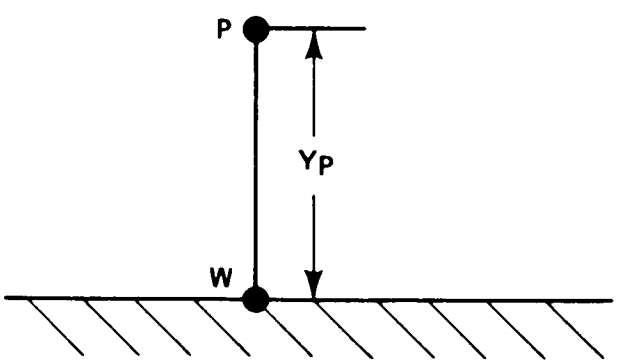

Figure 1. The near-wall model.

3.4 Reynolds Stress Models

The two equation models which have been extensively used in engineering calculations have several limitations. The main practical limitation is the assumption of isotropic eddy viscosity. The same values of ν_t are taken for different $\overline{u_i u_j}$ terms. The effects of curvature, rotation and buoyancy forces have to be modeled separately. In the models discussed so far the local state of turbulence is assumed to be characterized by one velocity scale $\sqrt{k}$. The individual $\overline{u_i u_j}$ is related to this scale. In actual flows, the scales may develop quite differently. In order to account for the different development of the individual stresses, transport equations for $\overline{u_i u_j}$ have been introduced. These equations can be derived in exact forms but they contain higher order correlations that have to be approximated in order to obtain a closed system. In this model one needs to solve the equation for the turbulence energy dissipation rate ϵ, in addition to those for $\overline{u_i u_j}$ for the length scale. A particular advantage of the Reynolds stress model is that terms accounting for buoyancy, rotation and other effects are in principle introduced automatically. However, many problems arise in the solutions of the model equations as discussed below and in Section 3.4.1.

Models employing transport equations for $\overline{u_i u_j}$ are called second order closure models. Several closure schemes have been proposed. The well tested one is that of Launder, et al. [23].

Launder et al. proposed the following model transport equations for $\overline{u_i u_j}$

$$\frac{\partial \overline{u_i u_j}}{\partial t} + U_l \frac{\partial \overline{u_i u_j}}{\partial x_l} = C_s \frac{\partial}{\partial x_l}\left(\frac{k}{\epsilon}\overline{u_k u_l}\frac{\partial \overline{u_i u_j}}{\partial x_k}\right) - \overline{u_i u_l}\frac{\partial U_j}{\partial x_l} - \overline{u_j u_l}\frac{\partial U_i}{\partial x_l}$$

Convective Transport; Diffusive Transport; p_{ij} = stress production

$$- C_1 \frac{\epsilon}{k}\left(\overline{u_i u_j} - \frac{2}{3}\delta_{ij} k\right) - C_2\left(P_{ij} - \frac{2}{3}\delta_{ij} P\right) - C_3\left(G_{ij} - \frac{2}{3}\delta_{ij} G\right)$$

Pressure Strain

$$- \beta\,(g_i u_j \phi + g_j u_i \phi) - \frac{2}{3}\epsilon\,\delta_{ij} \qquad (15)$$

Viscous Dissipation

G_{ij} = buoyancy production.

The rate of change, convective transport, and mean field as well as buoyancy production terms are exact whereas the diffusion, pressure-strain/scrambling, and viscous dissipation terms are model approximations. The diffusion fluxes of $\overline{u_i u_j}$ have been expressed by simple gradient diffusion models. Local isotropy has been assumed to prevail so that the dissipation is the same for all the three normal components (and thus 2/3 of the total dissipation ϵ) and, so that the viscous destruction terms for the shear stresses are zero. The most important assumption concerns the pressure-strain/scrambling terms,

since for shear stresses these are the main terms to balance the production of these quantities. The pressure-strain/scrambling model consists of three parts. The first one represents the interaction of fluctuating components only, the second the interaction of mean strain and fluctuating quantities and the third the effect of buoyancy forces. Several versions of the pressure strain model have been proposed to correctly predict the experimentally observed results. To account for the wall damping effects a wall correction must be introduced in the pressure-strain model. Launder et al. make the empirical constants in the pressure-strain model a function of the relative distance from the wall, $l/y \; \alpha \; k^{3/2}/(\epsilon y)$. Because of the complexity and the large amount of computational efforts required, the model has not been as widely used as one would like it to be.

3.4.1 Invariance and Realizability of Reynolds Stress Models

Turbulence models should be broad based so that they can be applied to most practical problems without "tuning." The Reynolds stress models come close to this ideal, since they account for more physical processes such as those due to curvature, rotation, buoyancy, etc. automatically. For general applicability, these models have to satisfy many constraints [17]. Of these constraints, tensor invariance and realizability seem to be important. The first one requires that the replaced terms have the same tensor form as the original terms. This will ensure that they transform properly in different coordinate systems. Such type of modeling is called invariant modeling [20]. The second constraint, realizability was first introduced by Schumann [24]. This condition requires that the equation for turbulent stresses have the property that all component energies remain non-negative and all off-diagonal components of Reynolds stress tensor satisfy Schwartz's inequality. These and the additional condition put forth by Schumann are written in a numerically most convenient form [24]:

$$R_{11} \geqslant 0 \quad , \tag{16}$$

$$R_{11} \, R_{22} - R_{12}^2 \geqslant 0 \quad , \tag{17}$$

$$R_{11} \, (R_{22} \, R_{33} - R_{23}^2) - R_{12} \, (R_{12} \, R_{33} - R_{23} \, R_{13}) + R_{13} \, (R_{12} \, R_{23} - R_{22} \, R_{13}) \geqslant 0 \quad . \tag{18}$$

Similar conditions apply for scalar fluxes. Schumann shows that the exact Reynolds stress equations satisfy the realizability condition. He also indicates the nonrealizability of some of the existing models. However, attempts to satisfy realizability conditions lead to invariably complicated model expressions [14]. Hence, at present no special efforts are taken to see that model equations satisfy realizability conditions. Care must be exercised in implementing and interpreting these models.

3.5 Algebraic Stress Model

In Reynolds stress models, there are differential transport equations for each component of $\overline{u_i u_j}$ in addition to ϵ equation. To reduce the computational effort, Rodi [25] proposed an algebraic relation for calculating the Reynolds stresses. The convection and diffusion terms in the transport equations of $\overline{u_i u_j}$ are replaced by model approximations, reducing the equations to algebraic equations. Rodi assumes that the transport of $\overline{u_i u_j}$ is proportional to the transport of k and that the proportionality factor is $\overline{u_i u_j}/k$. With this approximation incorporated, the transport equations yield algebraic expressions for

$\overline{u_i u_j}$ that contain the various production terms appearing in the $\overline{u_i u_j}$ equations. Thus the gradient of mean flow quantities, k and ϵ appear also in the expressions, so that k and ϵ equations have to be added in order to complete the turbulence model. The algebraic expressions together with k and ϵ equations form an extended k-ϵ model.

Algebraic stress models are suitable whenever the transport of $\overline{u_i u_j}$ is not important. Algebraic stress relations are basically like eddy viscosity formulations [15] and therefore are not applicable to cases where countergradient transports occur (Section VII). On the other hand, all effects that enter the transport equations for $\overline{u_i u_j}$ through the source terms for example, body force effects (buoyancy, rotation and streamline curvature), nonisotropic strain fields and wall damping influence can be incorporated. Algebraic stress models can therefore also simulate many of the flow phenomena that were described successfully by stress equation models.

3.6 Multiple-Scale Models

All the turbulence models discussed so far are based on the assumption that in all the flow situations each variable has a spectrum of universal form which can be characterized by the scales of the energy containing range. Difficulties arise when the spectrum is not an equilibrium one or when the flow exhibits distinctly different ranges of scales. Complex models have been devised to predict such flows [17]. The model of Hanjalic, et al. [26] appears to be a tractable and useful one. They split the spectrum into a large scale part and a small scale part with different time scales for transfer into the large scale part and transfer of the large scale part to the small scale part. A brief description of their model is given below.

The turbulence spectrum consists of independent production, inertial and dissipation ranges. K_1 denotes the wave number above which a significant mean strain production occurs while K_2 is the largest wave number at which viscous dissipation of turbulence is unimportant (Fig. 2). Energy leaves the first region (production) at a rate ϵ_p and enters the high wave number or dissipation region at a rate ϵ.

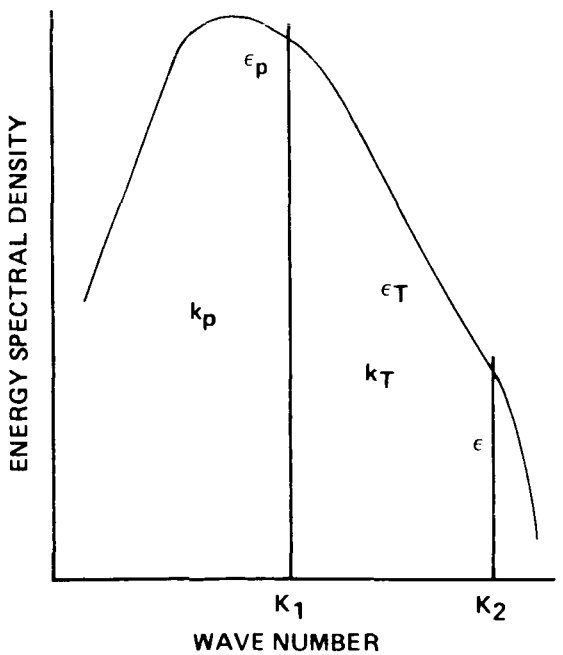

Figure 2. The spectral division for multiple scale model [26].

Between the two regions, occupying the intermediate range of wave numbers is the transfer region, across which a representative spectral energy transfer rate ϵ_T is assumed. This simplified energy spectrum is the basis of Hanjalic et al.'s model.

The total turbulence energy k is assumed to be divided between the production range k_p and the transfer range k_T. At high Reynolds numbers there is negligible kinetic energy in the dissipation range. In a homogeneous flow the levels of k_p and k_T are controlled by the transport equations,

$$\frac{Dk_p}{Dt} = \underbrace{-\overline{u_i u_j}\frac{\partial U_i}{\partial x_j}}_{P_k} - \epsilon_P \quad , \tag{19}$$

$$\frac{Dk_T}{Dt} = \epsilon_p - \epsilon \quad , \tag{20}$$

where P_k denotes the production rate of turbulence energy by mean shear which is assumed to be contained in the wave numbers below K_1. The following equations have been proposed for characterizing the evolution of these transfer rates.

$$\frac{D\,\epsilon_1}{Dt} = C_{\epsilon 1}\,P_k\,\frac{\epsilon_1}{k} - \frac{\epsilon_1^{\,2}}{k}\,(C_{\epsilon 2} + C_{\epsilon 3}\,A) + D_{\epsilon 1} \quad . \tag{21}$$

The quantity "A" refers to the turbulence anisotropy defined as

$$(\overline{u_i u_j} - 2/3\ \delta_{ij}\ k)\ (\overline{u_i u_j} - 2/3\ \delta_{ij}\ k)\ /\ k^2 \quad .$$

with $C_{\epsilon 1}$, $C_{\epsilon 2}$ and $C_{\epsilon 3}$ are constants determined from experiments. $D_{\epsilon 1}$ denotes the diffusive transport [equation (21) is for single scale model]. Equation (21) makes the local rate of ϵ_1 dependent on the local mean strain rate and the anisotropy of the stress field neither of which under conditions of local isotropy can directly affect the dissipation rate. Equation (21) may be regarded as a spectral energy transfer associated with large scale interactions. The proposed ϵ_p equation is:

$$\frac{D\,\epsilon_p}{Dt} = C_{P1}\,P_k\,\frac{\epsilon_P}{k_p} - C_{P2}\,\frac{\epsilon_P^{\,2}}{k_P} + D_{\epsilon p} \tag{22}$$

where the partioned energy k_p replaces the total energy giving, as the characteristic time scale, the turnover time of the large scale motions. C_{P1} and C_{P2} are constants.

The proposed form of the ϵ_T transport equation is

$$\frac{D\epsilon_T}{Dt} = C_{T1}\frac{\epsilon P \epsilon_T}{k_T} - C_{T2}\frac{\epsilon_T^2}{k_T} + D_{\epsilon_T} \tag{23}$$

C_{T1} and C_{T2} are constants determined from experiments. Energy dissipation rate now responds only slowly to the applied mean strain. This feature makes the form (23) more capable of representing the rapidly changing fields than equation (21). Hanjalic et al. computed the self-preserving plane and axisymmetric jets with this model using simple turbulent viscosity hypothesis for the shear stress $\overline{uv}$. They obtained very good agreement of the spread rates of the jets with the experimental values.

We have given here a brief account of various turbulence models along with their main features. Second order models and the models for two phase flows are not considered here. In the next section we discuss the corrections made to the widely used two-equation model to extend its applicability.

IV. MODIFICATIONS TO k-ϵ MODEL

Of all the models discussed in Section III, the two-equation, k-ϵ model has been widely used to predict various classes of flows of engineering importance. It has been used for predicting flows with heat/mass transfer, streamline curvature, etc. These effects have been accounted for by correcting the model equations. The low Reynolds number modification, wall-layer models and the streamline curvature corrections are discussed here.

4.1 Low-Reynolds Number Model

Jones and Launder [27] extended the k-ϵ model to low-Reynolds numbers so that the turbulence model equations can be valid throughout the laminar, transition and fully turbulent regions. In this version of the model, k and ϵ are determined from the following pair of equations.

$$\frac{D\epsilon}{Dt} = \frac{1}{\rho}\frac{\partial}{\partial x_j}\left[\left(\frac{\mu_t}{\sigma_\epsilon} + \mu\right)\frac{\partial \epsilon}{\partial x_j}\right] + C_1\frac{\epsilon}{k}\frac{\mu_t}{\rho}\frac{\partial U_j}{\partial x_j}\left(\frac{\partial U_i}{\partial x_j} + \frac{\partial U_j}{\partial x_i}\right) - \frac{C_2\,\epsilon^2}{k} - 2.0\,\frac{\nu\mu_t}{\rho}\left(\frac{\partial^2 U_i}{\partial x_j\,\partial x_1}\right)^2 \tag{24}$$

$$\frac{Dk}{Dt} = \frac{1}{\rho}\frac{\partial}{\partial x_j}\left[\left(\frac{\mu_t}{\sigma_k} + \mu\right)\frac{\partial k}{\partial x_j}\right] + \frac{\mu_t}{\rho}\frac{\partial U_i}{\partial x_j}\left(\frac{\partial U_i}{\partial x_j} + \frac{\partial U_j}{\partial x_i}\right) - 2\,\nu\left(\frac{\partial k^{1/2}}{\partial x_j}\right)^2 - \epsilon \tag{25}$$

In these equations, C_1, σ_k and σ_ϵ retain the values assigned to them for high Reynolds numbers while C_μ and C_2 vary with turbulence Reynolds number.

$$C_\mu = C_{\mu\infty}\exp\left[-2.5/(1 + R_t/50)\right] \quad , \tag{26}$$

$$C_2 = C_{2\infty} [1 - 0.3 \exp(-R_t^2)] \quad , \tag{27}$$

subscript ∞ refers to fully turbulent values. We note here, that the laminar diffusive transport becomes of increasing importance as the wall is approached and the extra destruction terms included are of some significance in the viscous and transitional regions. The term $2.0\, \nu\mu_t/\rho\, (\partial^2 U_i/\partial x_j \partial x_l)^2$ in the ϵ equation produces satisfactory variation of k with distance from the wall. The measurements indicate that the level of energy dissipation rate is constant in the immediate neighborhood of the wall. In the computations ϵ is set to zero at the wall and an extra term, $-2\nu\, (\partial k^{1/2}/\partial x_j)^2$ is introduced to the k equation. This extra term is exactly equal to the energy dissipation rate in the neighborhood of the wall.

4.2 Near-Wall Models

4.2.1 Two-Layer Model of Chieng and Launder

Detailed modeling of the near wall region is necessary for better prediction of the flow field. Recently Chieng and Launder [28] introduced detailed near wall modeling in their computation of flow in a pipe expansion. Their model is briefly discussed here. Figure 3 shows a scalar node P whose associated volume is bounded on the south side by a wall. The near wall flow is treated as viscous (but not laminar) out to a distance y_v from the wall and fully turbulent beyond this. The sublayer thickness y_v is such that the Reynolds number $y_v\, k_v^{1/2}/\nu$ $(= R_v)$ is constant, taken equal to 20. The near wall cell is large enough that the node P lies outside the viscous sublayer. Over the fully turbulent region the mean velocity parallel to the wall is assumed to vary with the distance from the wall according to

$$U\, k_v^{1/2}/(\tau_w/\rho) = \frac{1}{\kappa^*} \ln E^* \frac{y\, k_v^{1/2}}{\nu} \quad . \tag{28}$$

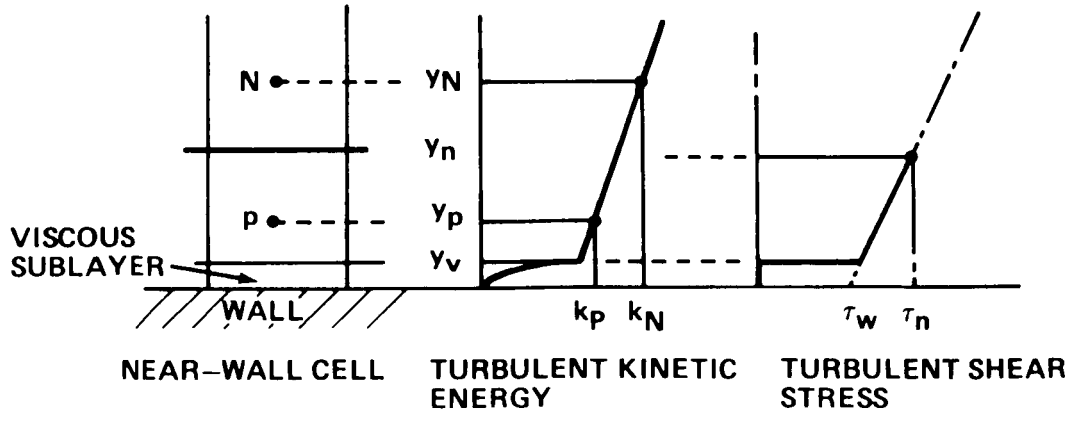

Figure 3. Near-wall two-layer model.

An expression for τ_w can be written in terms of U_p:

$$\tau_w = \frac{\kappa^* \rho U_P k_v^{1/2}}{\ln E^* y_P k_v^{1/2}/\nu} \quad . \tag{29}$$

The equations (28) and (29) are the same as the low Re version of Launder and Spalding [21] except that the kinetic energy term is evaluated here, at the edge of the viscous sublayer, rather than at node P. The κ^* in equation (28) is proportional to the von Karman constant κ. In local equilibrium, where $k = (\tau_w/\rho)\ C_{\mu\infty}^{-1/2}$ the velocity relation should reduce to the conventional logarithmic law:

$$U/\sqrt{\tau_w/\rho} = \frac{1}{\kappa} \ln E \frac{y\sqrt{(\tau_w/\rho)}}{\nu} \quad . \tag{30}$$

The limiting form is achieved by taking $\kappa^* = \kappa\ C_{\mu\infty}^{1/4}$ (0.23) and $E = E^*\ C_{\mu\infty}^{-1/4}$. The constant E^* can be evaluated in terms of R_v by noting that within the viscous sublayer the velocity displays a linear variation which may be written as

$$\frac{U k_v^{1/2}}{(\tau_w/\rho)} = \frac{y k_v^{1/2}}{\nu} \tag{31}$$

At y_v we find that $E^* = \exp(\kappa^* R_v)/R_v$. Thus for the assumed values of κ^* and R_v, $E^* = 5.0$.

The linear variation between the node P and its neighbor (point N) is used to extrapolate to the viscous sublayer (i.e., k_v in terms of k_P and k_N). Within the viscous sublayer a parabolic variation of kinetic energy is assumed.

$$k = k_v(y/y_v)^2 \quad . \tag{32}$$

This corresponds to the linear increase of the fluctuating velocity with distance from the wall.

The dominant contribution to the energy generation rate is the term $\tau_T\ \partial u/\partial y$, the τ_T is the local shear stress. The mean generation rate per unit volume is

$$1/y_n \int_{y_v}^{y_n} [\tau_w + (\tau_n - \tau_w)\ y/y_n] \frac{\partial U}{\partial y}\, dy \quad . \tag{33}$$

Using equation (30) for the mean velocity distribution

$$\text{Mean generation rate} = \frac{\tau_w(U_n - U_v)}{y_n} + \frac{\tau_w\,(\tau_n - \tau_w)}{\rho\,\kappa^*\,k_v^{1/2}\,y_n}\left(1 - \frac{y_v}{y_n}\right) \quad . \tag{34}$$

Unlike the generation, the dissipation rate of turbulence energy is not zero in the sublayer. It is constant equal to $2\nu\,(\partial k^{1/2}/\partial y)^2$. Using equation (25) we obtain

$$\epsilon = \frac{2\nu\,k_v}{y_v^2} \quad . \tag{35}$$

The mean value of the dissipation rate can be obtained by integrating (35) between y_v and y_n.

4.2.2 Two- and Three-Layer Models of Amano

Amano's near wall model [29] is the same as that of Chieng and Launder, except for the treatment of the generation and destruction terms in the ϵ equation. In Reference 28 the value of ϵ in the near wall cell was approximated under local equilibrium condition. Amano develops the treatment of the ϵ equation near the wall cell, taking into account that the value of ϵ near the wall is an order of magnitude larger than that in the fully turbulent core, and reaches its maximum at the wall. Each term in the ϵ equation should be evaluated in accordance with the k equation rather than approximated under local equilibrium conditions. He has considered both a two layer model and a three layer model. In the two layer model the region is divided into two distinct parts: a viscous sublayer region ($0 < y^+ < 11$) and an overlap region ($11 < y^+ < 400$). The ϵ equations for these regions have been developed [29].

In the three layer model he tries to approximate the experimental velocity profile more closely by dividing the near wall region into three layers: a viscous sublayer ($0 < y^+ < 5$) adjacent to the wall; a buffer layer ($5 < y^+ < 30$); and an overlap layer ($30 < y^+ < 400$) (Fig. 4).

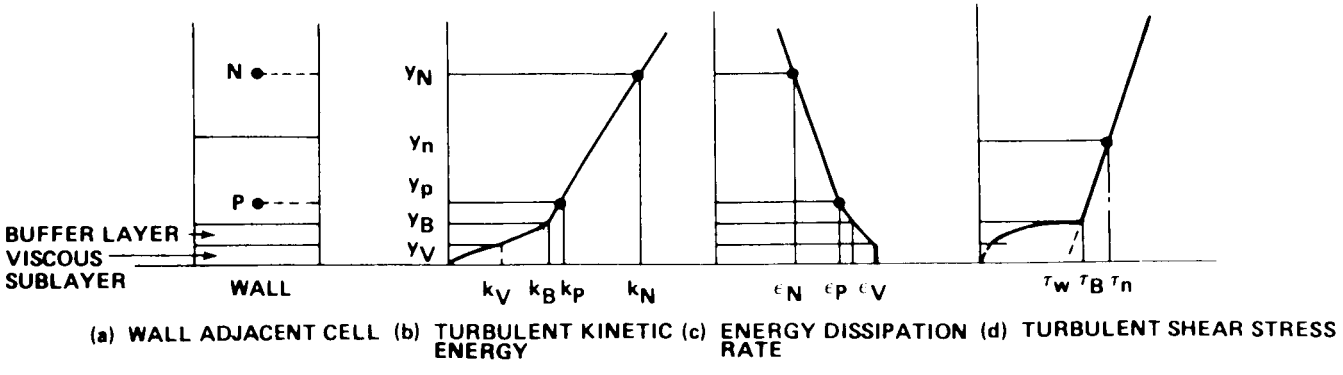

Figure 4. Near-wall three-layer model [29].

He assumes the following variation of k, ϵ and τ in the three regions:

Viscous Sublayer $0 < y^+ < 5$

$$k = k_v \, (y/y_v)^2$$

$$\epsilon = 2\nu \left(\frac{\partial k^{1/2}}{\partial y} \right)^2$$

$$\tau = 0 \quad . \tag{36}$$

Buffer Layer ($5 < y^+ < 30$):

$$k = k_B \, y/y_B$$

$$\epsilon = k^{3/2}/C_l \, y$$

$$\tau = \tau_B \, (y/y_B)^3 \quad . \tag{37}$$

Fully Turbulent Region ($30 < y^+ < 400$):

$$k = \frac{k_n - k_B}{y_n - y_B} y + \left(k_P - \frac{k_P - k_N}{y_P - y_N} y_P \right) = by + a$$

$$\epsilon = k^{3/2}/C_l \, y$$

$$\tau = \tau_w + (\tau_n - \tau_w) \, y/y_n \quad . \tag{38}$$

where

$$a = k_P - \frac{k_P - k_N}{y_P - y_N} y_P$$

$$b = \frac{k_n - k_B}{y_n - y_B} \quad .$$

He obtains the mean generation and destruction rates for k and ϵ equations, incorporating the above relations. He claims to obtain better results with these near wall models, the three layer model being superior to the two layer one.

The near-wall models of Amano and Chieng and Launder have been useful for improving the prediction of wall heat transfer rates. However, it appears that these models do not improve significantly the flow field predictions. For example, the models have little effect on the prediction of the location of the reattachment point [28] (also, see Section V).

4.2.3 PSL Approach

In an attempt to model the physics of near wall region, Iacovides and Launder [30] have recently proposed a numerical scheme which employs the classical boundary layer assumption for the thin wall layer and eliminates the use of wall functions. In this approach a thin parabolic sublayer (PSL) near the wall is assumed across which static pressure variation is either negligible, or if the surface is highly curved, can be obtained assuming radial equilibrium. The PSL is taken to extend over the whole low Re region where the transport coefficients vary by orders of magnitude. A fine computational grid treatment for this layer eliminates the use of wall functions. In PSL approach no pressure need be computed or stored at the grid points within the layer and the velocity component normal to the wall at these node points are obtained by cell continuity rather than solving the normal momentum equation. Iacovides and Launder employ a staggered arrangement of dependent variables as shown in Figure 5, and the normal component of velocity evaluated from

$$V(I,J) = [U(i-1,J) - U(I,J)]\,\delta y/\delta x + V(I,J-1) \quad . \tag{39}$$

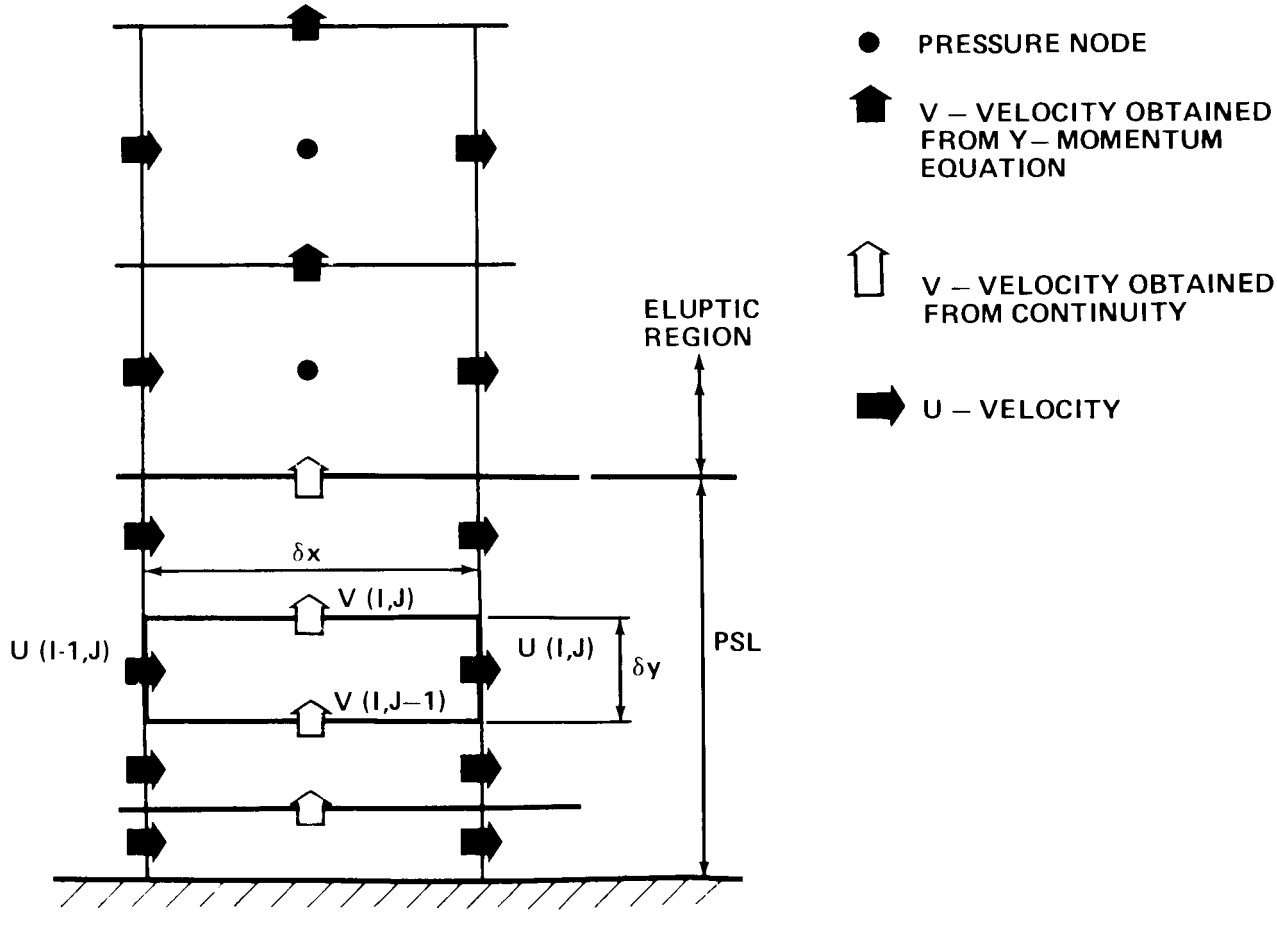

Figure 5. PSL approach [30].

The PSL approach has been successfully used for computations of flow and heat transfer in a pipe expansion, in a spirally fluted tube and in a 90 deg tube bend by Launder [31]. It has been found that the PSL approach is not only as economical as the wall function approach to obtain grid independent solutions, but also produces more realistic solutions. For example, in the flow in a pipe expansion, the PSL approach reveals a secondary recirculation region, not produced by the wall function method, for high expansion ratios [31]. The secondary recirculation region accounts for the Nusselt number variations downstream of the expansion observed in the experiments.

4.3 Curvature Effects

An exhaustive review of the subject and many insights into the effects of streamline curvature on turbulence and ways of incorporating into the turbulence models were provided by Bradshaw [32]. Large changes in Reynolds stress observed in the curved flow experiments cannot be accounted for by the extra terms appearing in the mean flow and Reynolds stress transport equations. Streamline curvature causes large changes in higher order quantities (second order) of the turbulence structure. Effects are similar when the streamlines have a component of curvature in the plane of mean shear irrespective of the cause of the curvature, caused by surface curvature or swirl or rotation of the whole system. Since the models can recognize only the explicit extra terms due to curvature in the mean motion and turbulent transport equations, they will severely underpredict the effects. Hence, the models have to be modified to account for the curvature effects.

Modifications to the k-ϵ model have been made to incorporate the streamline curvature caused by surface curvature as well as by swirl or rotation. The modification of the length scale suggested by Bradshaw is employed in most computations. It is made a linear function of the curvature Richardson number. Another way of incorporating the curvature effect is through the modification of C_μ. For the convenience of discussions on model predictions in Section V, the modifications employed in the flows with surface curvature and in the flows with swirl are given here separately.

4.3.1 Flows with Surface Curvature

Gibson [33] derived a set of algebraic stress equations from which the effect of curvature on mixing length and turbulent Prandtl number can be obtained. His analysis was, however, limited to moderate curvatures. Following the idea of Gibson, Pourahmadi and Humphrey [34] studied the effect of curvature for any arbitrary curvature. They obtain a general expression for C_μ by equating the algebraic expression derived for $u_\theta u_r$ with the Boussinesq approximation for $u_\theta u_r$ in which μ_t is given by

$$\mu_t/\rho = C_\mu \, (k^{3/2}/\epsilon) \, k^{1/2} \quad .$$

They use the expression derived for C_μ in the k-ϵ model equations. The variation of C_μ for a curved channel obtained by them is shown in Figure 6.

The figure shows the variations of C_μ as a function of radial position in channels of different curvature. In general, C_μ is seen to increase at both walls of a curved channel at a rate inversely proportional to the channel curvature (R_c/D). For strong curvatures they obtained unrealistic values of the

parameter in the region $0.3 \leqslant r \leqslant 0.65$ due to the lack of consistency of the ratio $\overline{u_i u_j}/k$. They used the fixed values of $C_\mu = 0.09$ in the region $0.3 < r < 0.65$.

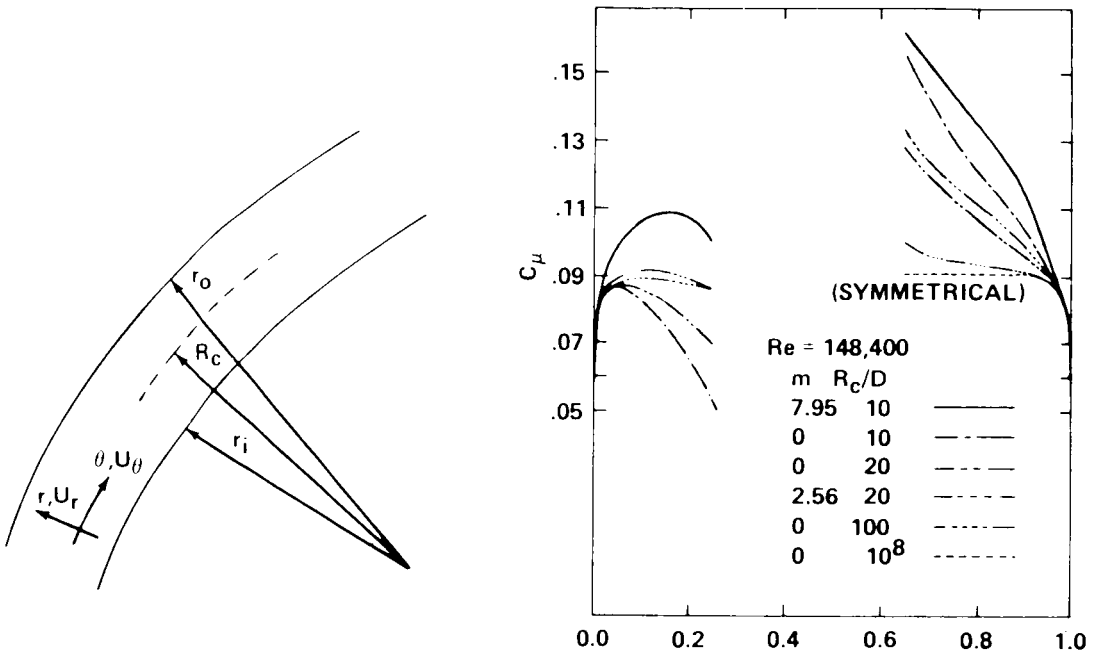

Figure 6. Surface curvature: geometry and variation of C_μ for fully developed curved and straight channel flow [34].

The relative importance of wall curvature and wall pressure fluctuations on C_μ have been shown by two sets of C_μ profiles (R_c/D = 10 and 20) with imposed (m=0) symmetric wall functions of f equivalent to the straight channel flows in so far as the wall pressure corrections are concerned, while retaining the direct influence of wall curvature on C_μ. The C_μ profiles show that, the curvature at the concave wall acts to enhance while the curvature at the convex wall acts to suppress it. The inclusion of wall pressure corrections in the pressure strain (m = 2.56 and m = 7.95) further increases C_μ at both the walls, but at the convex wall the direct influence of curvature effects ultimately dominate the wall pressure contributions to C_μ causing a net decrease in its value with increasing distance from the wall.

Launder et al [35] introduce corrections to the length scale determining ϵ-equation to account for curvature effects. The constant C_2 is made to depend on the gradient Richardson number defined as

$$R_i = \frac{k^2}{\epsilon^2} \frac{W}{r^2} \frac{\partial(rW)}{\partial r} \quad . \tag{40}$$

They solve the following form of k-ϵ equations in addition to the mean flow equations for two dimensional curved duct flows.

$$\rho U \frac{\partial k}{r\partial\theta} + \rho V \frac{\partial k}{\partial y} = \frac{1}{r}\frac{\partial}{\partial y}\left(r\left(\mu + \frac{\mu_t}{\sigma_k}\right)\frac{\partial k}{\partial y}\right) + P_k - \rho\epsilon - 2\mu\left(\frac{\partial k^{1/2}}{\partial y}\right)^2 \tag{41}$$

$$\rho U \frac{\partial \epsilon}{r\partial\theta} + \rho V \frac{\partial \epsilon}{\partial y} = \frac{1}{r}\frac{\partial}{\partial y}\left(r\left(\mu + \frac{\mu_t}{\sigma_\epsilon}\right)\frac{\partial \epsilon}{\partial y}\right) - C_1 \frac{\epsilon}{k} P_k - C_2 \rho \frac{\epsilon^2}{k}(1 - C_c R_i) - C_2 \nu\mu_t\left(\frac{\partial^2 U}{\partial y^2}\right)^2 \tag{42}$$

where

$$P_k = \mu_t\left(r\left(\frac{\partial U}{r}\right)/\partial y\right)^2 \quad .$$

The new constant introduced C_c for curvature varied from 0 to 0.5.

The influence of curvature can also be accounted for by modifying the velocity scale. Since velocity scale effects are included in k-equation such modifications have not been very useful [36-38]. Lilley [39] includes the effects of curvature in kl equation by an additional term in his k-kl two equation model.

4.3.2 Flows With Swirl

For flows with swirl, the k-ϵ model is varied in a simple way by introducing corrections to the length scale determining ϵ-equation. There are two corrections in use. One is to modify the constant C_2 appearing in the sink term and the other is to modify the constant C_1 appearing in the source term of the ϵ-equation, by relating them to the Richardson number. However, the form of the Richardson number used in the two cases are different. The term C_2 is corrected using the gradient Richardson number R_i given by equation (40) [40,41,35]. For example, Launder et al. [29] replace C_2 by

$$C_2 = 1.92\,(1 - 0.2\,R_i) \quad . \tag{43}$$

Srinivasan and Mongia [41] split R_i into two parts: (i) swirl Richardson number, equation (40), and (ii) curvature Richardson number defined below, in an arbitrary way. They represent C_2 as

$$C_2 = 1.92 \exp(2\alpha_s R_i + 2\alpha_c R_{ic}) \tag{44}$$

$$R_{ic} = \sqrt{U^2 + V^2}\ / R_c\left[\frac{1}{r}\frac{\partial}{\partial r}(rU) + \frac{\partial V}{\partial x}\right] \tag{45}$$

where the radius of curvature is given by

$$(1/R_c) = \frac{UV\,[1/r\;\partial/\partial r\;(rU) - (\partial U/\partial x)]}{(U^2 + V^2)^{3/2}} \quad . \tag{46}$$

The values of α_s and α_c were arrived at by parametric studies, to be $\alpha_s = -0.75$ and $\alpha_c = -2.0$.

Rodi [42] is probably the only one employing the correction to C_1 by relating it to the flux Richardson number R_f

$$R_f = \frac{2W\,\dfrac{\partial W/r}{\partial r}}{2\left[\left(\dfrac{\partial U}{\partial x}\right)^2 + \left(\dfrac{\partial V}{\partial r}\right)^2 + \left(\dfrac{V}{r}\right)^2\right] + \left(\dfrac{\partial U}{\partial r} + \dfrac{\partial V}{\partial x}\right)^2 + \left(\dfrac{\partial W}{\partial r}\right)^2 + \left[r\,\dfrac{\partial}{\partial r}\left(\dfrac{W}{r}\right)\right]^2} \tag{47}$$

He represents C_1 as

$$C_1 = 1.44\,(1 + 0.9\,R_f) \quad . \tag{48}$$

This form of correction has been found to produce the destabilizing effect of rotation on turbulence in swirl flows correctly. The use of R_f is to be preferred for flows with swirl for the following reasons:

(i) It represents correctly the effect of rotation on turbulence.

(ii) It is the only suitable parameter for three dimensional flow analysis.

(iii) It reduces to gradient Richardson number when the curvature is small.

The curvature effects may, however, be taken care of automatically, if one uses transport equations for turbulent shear stresses.

The applications of the various turbulence models and the model varients discussed here to internal flow predictions are discussed in detail in the following section.

V. APPLICATIONS OF TURBULENCE MODELS TO THE PREDICTION OF INTERNAL FLOWS

The geometrical configuration, the fluid and the flow rate all determine the complexity of the flow. For any combination of these factors, one is interested in a prediction method to obtain information on pressure drop, flow pattern, temperature distribution, etc. This paper is concerned here with the computation of turbulent flows via the solution of time averaged Navier-Stokes equations for a set of flows of engineering interest. Turbulence closure models and their prediction capabilities will be considered. In the 1981-Stanford conference on complex turbulent flows [43] several isothermal flows

of engineering interest were computed and compared with carefully compiled experimental data. This included a number of confined flows, which they classified into two groups: (i) attached flows and (ii) separated flows. Here, the application of turbulent closure models to a selected set of flows of interest is discussed and the performance of the models is evaluated.

Precise comparison of the performance of closure models is difficult because of the difference in numerical schemes used. Turbulence models and numerical methods are considered independent elements of the total turbulent flow computation. In principle, one can solve any set of turbulence model equations with any numerical method. In practice, when the agreement between the computed and experimental results is not so good, one is not sure where to put the blame; i.e., turbulence model or the numerical method; many tend to blame the turbulence model, because of the faith in their numerical method. Hence, an evaluation of the turbulence closure models rests mainly on their predicted flow quantities of engineering interest (such as the size of the recirculating flow, profiles of velocity, pressure, kinetic energy, etc.) and their closeness to the experimental or expected results.

In this section, an attempt is made to catalog recent applications of turbulence models to confined flows under the following classes:

5.1 Plane two-dimensional computations

(a) Backward facing step flow
(b) Symmetric expansion
(c) Flow over a square obstacle.

5.2 Axisymmetric two-dimensional computations

(a) Flow in a sudden pipe expansion
(b) Diffuser flows
(c) Flows with curvature and swirl

5.3 Three-dimensional computations

Non-circular duct flows

In each class, the predictions by various turbulence models are compiled and the major predicted quantities are compared. Some observed discrepancies between the prediction and experiment are discussed.

5.1 Plane Two-Dimensional Flows

5.1.1 Backward Facing Step Flow

The flow over a backward facing step (Fig. 7) was a bench mark problem in the 1981-Stanford Conference: flow No. 0421. The results of different turbulent models [44-50] are briefly reviewed here. Since we are interested in the recirculating flow, some special methods (which do not solve an elliptic equation) adopted for this problem are not included here. Recent results of Ilegbusi and Spalding [51], Nallasamy [52] and Syed et al. [53] are also included. Table 1 lists the turbulence models used by different authors and some observations.

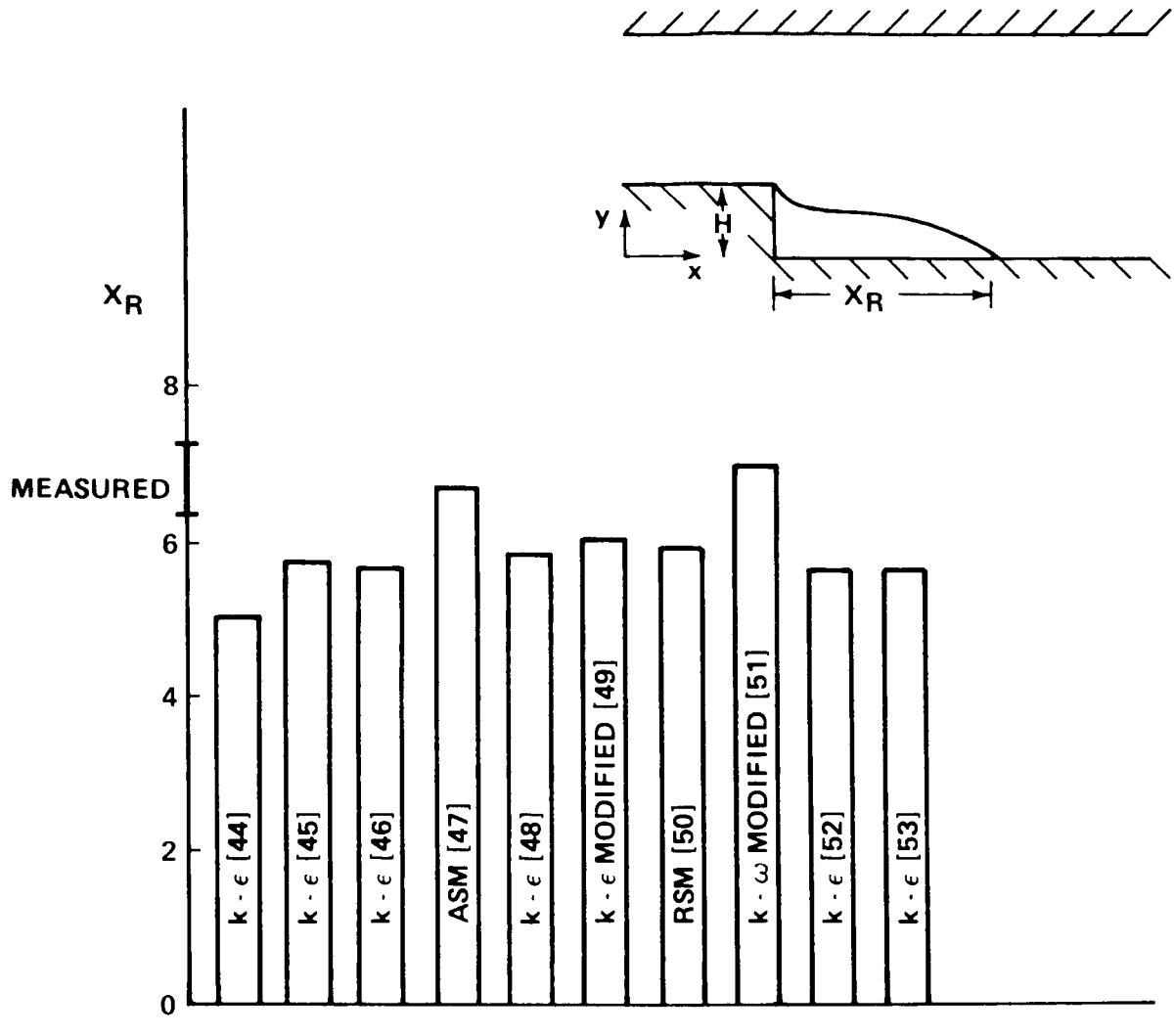

Figure 7. Flow over a backward facing step: predicted separation length, X_R.

A useful parameter for comparison in backward facing step flow is the length of the recirculation region x_R. Figure 7 gives the reattachment lengths predicted by different computations. The experimentally observed value of x_R is (7.0±0.5) step height [54]. Standard k-ϵ models underpredict the reattachment length by as much as 20 percent. Modified k-ϵ models [49,51], algebraic stress model [47] and Reynolds stress model [50] predict recirculation length fairly well. Demirdzic et al. [49] use the near wall model (Section 4.2) of Chieng and Launder [35] with the standard k-ϵ model, with modifications for the production and diffusion terms in the ϵ equation. This computation underpredicts the value of x_R by about 11 percent. It is observed that the better prediction of x_R is due to the modification of the diffusion and production terms to account for the streamline curvature. The recent study of Ilegbusi and Spalding [51], using the near wall treatment [28] and modified k-w model, predicts x_R which agrees with the experiments [54,55]. This model requires the specification of two additional constants. The exact reason for the underprediction of x_R by the standard model, however, is unclear (see Section 5.2.1).

All the methods overpredict the shear stress in the separated shear layer. This implies that in this region, the computed turbulent viscosity will be higher than that existing in an actual flow. This, of course, can result in a shorter reattachment length as observed in all the predictions. The redevelopment of the flow downstream of the reattachment is also not correctly predicted in any of the predictions.

TABLE 1. FLOW OVER A BACKWARD FACING STEP

Reference	Turbulence Model	Flow Properties Compared	Remarks
Mansour and Morel [44]	k-ϵ	Wall static pressure P Mean velocity $\overline{U}$ Shear stress $\overline{uv}$	x_R = 5.2 H Different near wall models have no effect on x_R
Pollard [45]	k-ϵ	p, $\overline{U}$, $\overline{uv}$	x_R = 5.88 H Reasonable agreement with cross stream $\overline{uv}$, poor prediction of axial variation of $\overline{uv}$
Rodi et al. [46]	k-ϵ	p, $\overline{U}$, $\overline{uv}$	x_R = 5.8 H Shear stress over predicted, recovery beyond reattachment not well predicted.
Launder et al. [47]	Algebraic stress model	p, $\overline{U}$, $\overline{uv}$	x_R = 6.9 H Agrees with the experimental result. Predicts a slower downstream development compared to experiment.
Spalding et al. [48]	k-ϵ	p, $\overline{U}$, $\overline{uv}$	x_R = 6 H
Demirdzic et al. [49]	Modified k-ϵ. Modifications to production and diffusion terms in ϵ equation. Near wall model of C and L [28]	p, $\overline{U}$, $\overline{uv}$	x_R = 6.2 H rate of growth of outer edge underpredicted. Effect of each of the two modifications is not known.
Donaldson et al. [50]	Reynolds stress model	p, $\overline{U}$, $\overline{uv}$	x_R = 6.1 H Prediction is good but expensive.
Ilegbusi and Spalding [51]	k-ϵ modified near wall model of C and L k-ω modified. new term added (two more constants) near wall model of C and L	p, $\overline{U}$, $\overline{uv}$	x_R = 7.2 H k-ϵ and k-ω predict equally well. Predicts the shear stress variation across the channel as well as along the channel reasonably accurately.
Nallasamy [52]	k-ϵ model	p, $\overline{U}$, $\overline{uv}$ Contours of k, ϵ	x_R = 5.8
Syed et al. [53]	k-ϵ Model	x_R	x_R = 5.8 (Low Re flow)

Ilegbusi and Spalding [51] with their modified k-ω model obtain a value of x_R = 7.2 H. Their conclusion, however, is that both k-ϵ and k-ω model (modified) predict the flow over a backward facing step equally well. The difference between the predicted and measured peak shear stress across the channel ranged from -17.5 percent to -1 percent for the k-ϵ model as compared to -4 percent to +21 percent for the k-ω model. Static pressure is well predicted by both the models.

Launder [56] discusses the effects of mesh size, false diffusion and inlet boundary conditions on the flow prediction. These are considered in Section VI.

There arises a question about the prediction of the flow over a backward facing step. Why is it that the flow in a pipe expansion is predicted well (Section 5.2.1) but not the asymmetrical channel expansion? One is reminded of the problem of the prediction of plane and axisymmetric jet flows [57,58], where the spreading rate of a plane jet is correctly predicted while that of an axisymmetric jet is overpredicted using the standard k-ϵ model. It is not exactly clear what causes this difference in predictions between the two confined flow geometries. An attempt is made to explain the behavior of the k-ϵ model in the two cases in Section 5.2.1.

5.1.2 Symmetric Expansion (Double Step) Flow

Gosman et al. [59] studied the plane symmetric sudden expansion (sometimes called a double step) flow using k-ϵ model. The regions of recirculation on both sides of the symmetric plane were identical for low expansion ratios. For large expansion ratios (>1.5), they observed that the two recirculation regions interact to produce asymmetric regions of recirculation. At some conditions, they observed two regions of recirculation on one side and one on the other side of the symmetric plane. The numerical results for the range of expansion ratios where symmetry was observed showed good agreement with experiments [60]. Though one would expect that the stabilizing effect of the top wall (instead of a symmetry line) to produce a shorter recirculation region in the case of asymmetric (single step) expansion flow as compared to double step flow, it has not been precisely measured in the experiments.

5.1.3 Flow Over a Square Obstacle

Durst and Rastogi [61] investigated theoretically as well as experimentally (using LDA) the flow over a square obstacle in a two-dimensional channel. They used a k-ϵ model and a three equation k, ϵ and $\overline{uv}$ model. They obtained a recirculation region behind the obstacle of size x_R = 7.5 H. The calculations showed reattachment on the obstacle itself (Fig. 8) which was not observed in the experiments. This they attribute to three-dimensional effects. Velocity profiles upstream were faithfully reproduced, while over and behind the obstruction the agreement was poor. The redevelopment after the reattachment was also slow. Use of the three equation model improves the calculated mean velocity profiles, but not significantly. The kinetic energy profiles show only qualitative agreement. The calculated length scales in the separated region and downstream of separation point indicate large scale eddies. They observed that the k-ϵ model has to be modified to obtain more accurate calculations in the separated region.

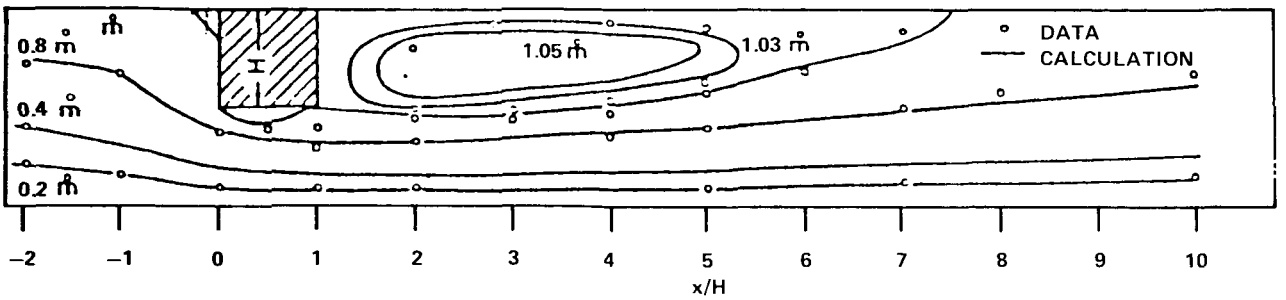

Figure 8. Flow over a square obstacle: predicted and measured flow pattern [61].

5.2 Axisymmetric Flows

5.2.1 Flow in a Sudden Pipe Expansion

Flow in a pipe expansion is one of the basic problems encountered in common engineering flow systems. The separated, reattached and recirculating flow downstream of the expansion greatly influences the transport of momentum and heat. Increased levels of heat and mass transfer occur. This increase is attributed to increase in levels of turbulent kinetic energy in the stream. The high kinetic energy comes about due to the large shear stress in the separated layer and the associated low rate of turbulent energy dissipation. Because of the intrinsic practical interest several experimental and theoretical studies have been carried out on this flow configuration. This geometry also forms the basic configuration for combustor studies (dump combustors), with swirl introduced before the expansion. In earlier computations of pipe expansion flow, a uniform length scale over the entire separated region was assumed [11]. Only with the introduction of a differential equation for calculating the variation of the length scale in the separated region, computations can predict the desired flow properties (Section 5.1).

As in the backward facing step flow, an important parameter for comparison of pipe expansion flow predictions, is the reattachment length x_R. The location of the reattachment point also determines the location of maximum heat/mass transfer coefficient. Figure 9 shows the predicted separation lengths by different computations. Table 2 lists the turbulence model used by different authors and some observations. The experimentally observed value of x_R is 8.5 to 9 H for this geometry [64,68,69]. From the figure one notices the following: In contrast to the predictions of backward facing step flow, the standard k-ϵ model predicts the reattachment length within the experimental uncertainty. This is interesting since it has some implications on the set of model constants used. One can discern the following prediction trends when one uses the same model constants appropriate for the boundary layer flows.

The flow in a sudden pipe expansion is predicted fairly well while the flow over a backward facing step is underpredicted by about 20 percent, using the standard k-ϵ model. It is not clear whether this is related to the problem of the prediction of plane and axisymmetric unconfined jet flows [57,58]. However, the underprediction of the flow over a backward facing step flow may be related to the underprediction of the recirculation region in the bluff-body stabilized flows [70]. Habib and Whitelaw [71,72] observe that the k-ϵ model connects the dissipation rate/production strongly to the mean flow field. In regions where there is more than one major component of velocity gradient tensor extra strain rates are added to the generation terms. Then, the Reynolds stresses change by values that are much larger than the direct effect of these strains and this is not represented by the effective viscosity model [32]. The response of the k-ϵ model to changes in mean flow field is too fast. The stabilizing effect of the top wall in the flow over a backward facing step may not be correctly represented in the k-ϵ model.

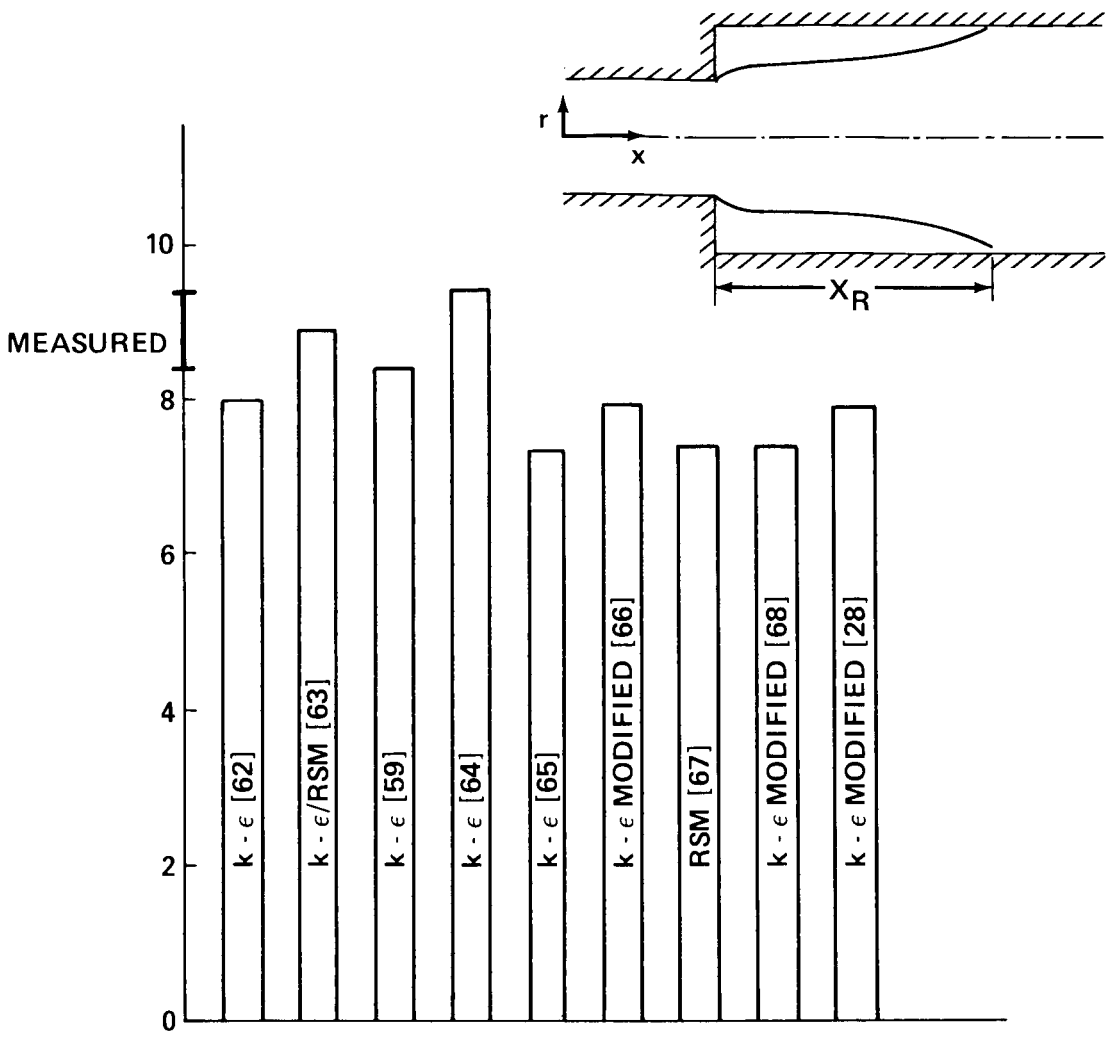

Figure 9. Axisymmetric expansion; predicted separation length, x_R.

Habib and Whitelaw [71] find that in the confined coaxial jet predictions, with the increase in the velocity ratio of annulus to pipe greater than unity, the underprediction of the separation region increases. The top wall in the backward step flow may have similar effects.

Reverting to Table 2, the modified k-ϵ models of References 66, 67, 68, and 28 do not appreciably improve the reattachment length. Chieng and Launder [28] state that the near wall model does not change the reattachment region but only improves the heat transfer prediction. The reduced value of x_R in these cases may be partly due to the low Reynolds number (R_{eD}) of these computations. Reference 64 gives the variation of x_R with R_{eD}.

To conclude this section, it is observed that no standard modification of the k-ϵ model which will respond correctly to the axisymmetric as well as asymmetric plane expansion flow has been arrived at. It appears that the algebraic stress model would be a better alternative.

TABLE 2. FLOW IN A SUDDEN PIPE EXPANSION

Reference	Turbulence Model	Computed Flow Properties	Remarks
Qin [62]	k-ϵ	$\overline{U}$, k, $\overline{uv}$	$x_R = 8$ H ($R_{eD} = 10^5$) Predictions fairly good in the reattachment region; beyond the reattachment region discrepancies between the prediction and experiment increases.
Ha Minh and Chassaing [63]	k-ϵ and RSM after reattachment	$\overline{U}$, $\overline{uv}$, p	$x_R = 9$H Predicted mean velocities and turbulent intensities agree well with the experiments.
Gosman et al. [59]	k-ϵ	P, $\overline{uv}$; contours of $\overline{U}$, k, and k/$\overline{uv}$	$x_R = 8.5$ H
Moon and Rudinger [64]	k-ϵ	Central line velocity size of the recirculation region	$x_R = 9.5$ H Slower decay of central line velocity, predicted recirculation region is thinner than the experimental one
Chen [65]	k-ϵ	p, $\overline{uv}$, $\overline{U}$, contours of k, ϵ	$x_R = 7.0$ H
Amano [66]	k-ϵ with near wall treatment (Sec. 4.2)	Nu	$x_R = 7.5$ to 8.5 H (estimated) Wall layer treatment improves the heat transfer prediction
Amano and Goel [67]	Reynolds stress model	Nu	$x_R = 7.0$ to 8.0 H (estimated) ($R_{eD} = 20000$) RSM predictions better than that of k-ϵ modified (wall treatment) RSM improves the prediction of heat transfer rates in the redevelopment region
Amano [68]	k-ϵ modified near wall model	Nu	$x_R = 7.0$ to 8.0 H (estimated) ($R_{eD} = 48000$)
Chieng and Launder [28]	k-ϵ modified (a) wall layer model (b) low Re model for near wall region	Nu	$x_R = 8$ H Computations show greater sensitivity to R_{eD}. Near wall model does not change the location of the maximum Nu_x (implies location of reattachment). Use of (b) produces unrealistic Nu values due to large length scales obtained near the wall.

5.2.2 Diffuser Flows

The axisymmetric diffuser flows can be divided into two groups: (i) small angle diffusers (no separation) with expansion of total angles equal to 5 to 10 deg, represent the aerodynamic diffusers; (ii) large angle diffusers (with separation) as found in "dump" combustors (90 deg half angle represents the sudden expansion). The computation of group (i) flows is generally through the solution of parabolic type equations and will not be considered here. In the second class only two recent contributions will be discussed.

Habib and Whitelaw [73] computed the axisymmetric recirculating flows in wide angle diffusers and compared this with their experimental results. They considered 20 and 40 deg half-angle geometries. The diameter expansion ratio was 2.0. They computed the flow with an orthogonal-curvilinear (body fitted) coordinate system. The standard k-ϵ model was employed. Mean axial velocity and radial velocity profiles and kinetic energy contours were presented and compared with experiments.

They find that the location of the maximum kinetic energy is correctly predicted but its value is underpredicted by about 30 percent. They attribute this to the incorrect representation of the source terms in the transport equation for ϵ and partly to the extra strain terms in the calculations of Reynolds stress terms and the rate of dissipation. The mean axial velocity and radial velocity are well predicted. Rhode et al. [74] report the computed results for expansion angles of 45, 70 and 90 deg, for the diameter expansion of 2. They use a non-uniform grid system and the standard k-ϵ model. The predicted mean velocity profiles show good agreement with the experiments of [69]. The computed flow pattern agrees with their flow visualization pictures. They characterize the size and shape of the recirculation region as a function of the angle of the sloping wall. They, however, did not make any comparison of the turbulence quantities such as the Reynolds stress.

5.3 Curved Flows

This section discusses the predictions of flows with streamline curvature caused by the surface curvature and swirl.

5.3.1 Flows with Surface Curvature

Pourahmadi and Humphrey [34], using their modifications for the value of C_μ discussed in Section 4.3, obtained very good predictions for the fully developed flow in a highly curved two-dimensional duct.

Figure 10 shows the streamwise variation of friction factor at the inner and outer walls of strongly curved channel flow. The use of standard C_μ in k-ϵ overpredicts the innerwall C_f while severely underpredicting the outer wall C_f. The modified model predicts the inner wall C_f very well and greatly improves the C_f at the outer wall. These predictions are in agreement with the experiments of Honami et al. [75]. The prediction of the mean velocity profiles is satisfactory even with standard k-ϵ models. Launder et al. [35] predicted the curved duct flow corresponding to the experiments of Ellis and Joubert [76], with the modification of lengthscale incorporating the gradient Richardson number. They obtain good agreement for the mean velocity and the shear stress at the inner wall.

Towne [77] has computed the turbulent flow through circular and square cross sectioned S-ducts using three-dimensional parabolic equations with marching procedure. He obtains good agreement of the

mean velocity profile with experiment, but no details of the shear stress variation is reported. He used an algebraic mixing length turbulence model. Typical streamwise velocity profiles in the pipe are shown in Figure 11. It is seen that a fine mesh (50 x 50 x 80) is needed to produce a meaningful prediction of the mean velocity profile variation.

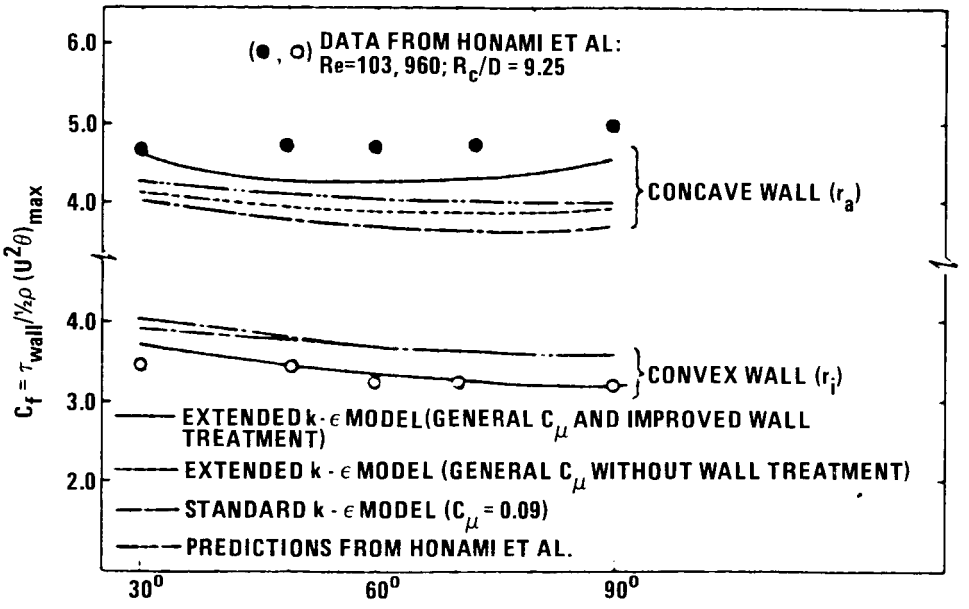

Figure 10. Streamwise variation of friction factor at the inner and outer walls of strongly curved channel flow [34].

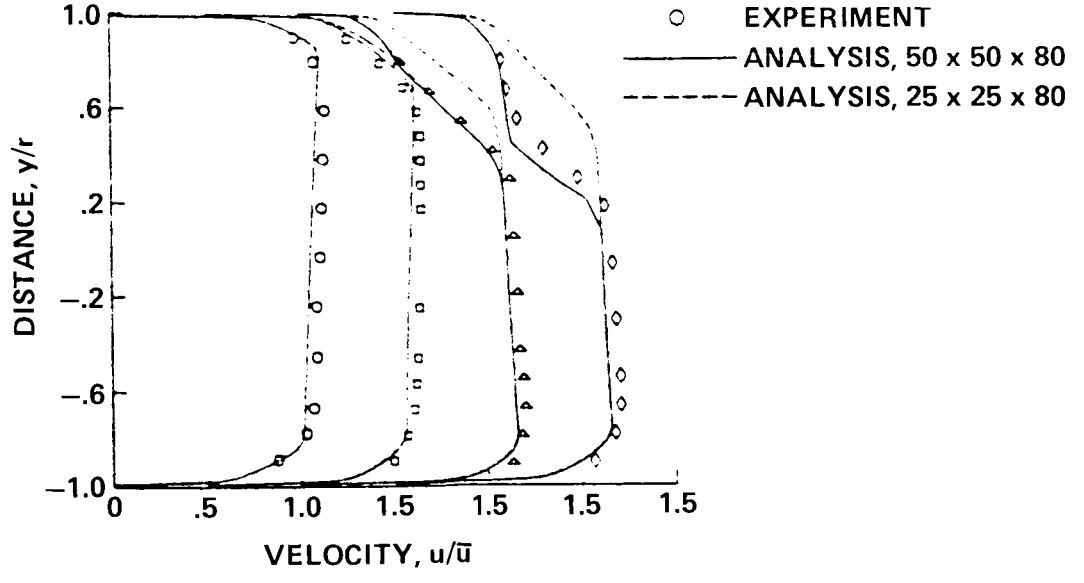

Figure 11. Computed and measured streamwise velocity profiles in symmetry plane for turbulent flow in 22.5 to 22.5 circular S-duct [77].

Mukerjee et al. [78] use the k-ϵ model to compute the flow in a highly curved 180 deg turnaround axisymmetric duct configuration of the SSME. The curvature effect has not been explicitly included in their turbulence model. Because of this, it is difficult to estimate the accuracy of the solution, though it appears to predict the trend qualitatively [79]. No detailed predictions of the turbulent flow in a highly curved channel has been reported in the literature. Agarwal et al. [80] using LDA obtained detailed laminar flow characteristics in a 180 deg curved tube, of R_c/r = 7 and 20. This flow was successfully simulated using a three-dimensional code with fine mesh (50 x 50 x 226) by Towne [77]. No detailed experimental results are available for the 180 deg bend of $R_c/r \approx 1$ as found in SSME turnaround ducts.

5.3.2 Flows with Swirl

Swirling flows result from the application of a tangential velocity component imparted to the flow by swirl vanes, tangential entry, etc. Swirl flow occurs in a variety of applications, the most extensively studied one being the combustion aerodynamics. Nuttal [81] was the first one to observe the reverse flow characteristics of a swirling flow in a circular pipe. For Reynolds numbers in the range 1×10^4 to 3×10^4, three types of flow patterns are observed as shown in Figure 12. Transition from one-celled to two and finally a three-celled vortex structure occurs, as the swirl component of the velocity increases. This would be a difficult problem for modeling. A compendium of experimental and computational studies of swirl flows can be found in the recent book, "Swirl Flows," by Gupta et al. [82]. The review by Jones and Whitelaw [83] provides a good account of the prediction methods for reacting flows. The following sections discuss predictions of two nonreacting swirl flow configurations, namely the swirl flow in a pipe expansion and the swirled confined coaxial jets.

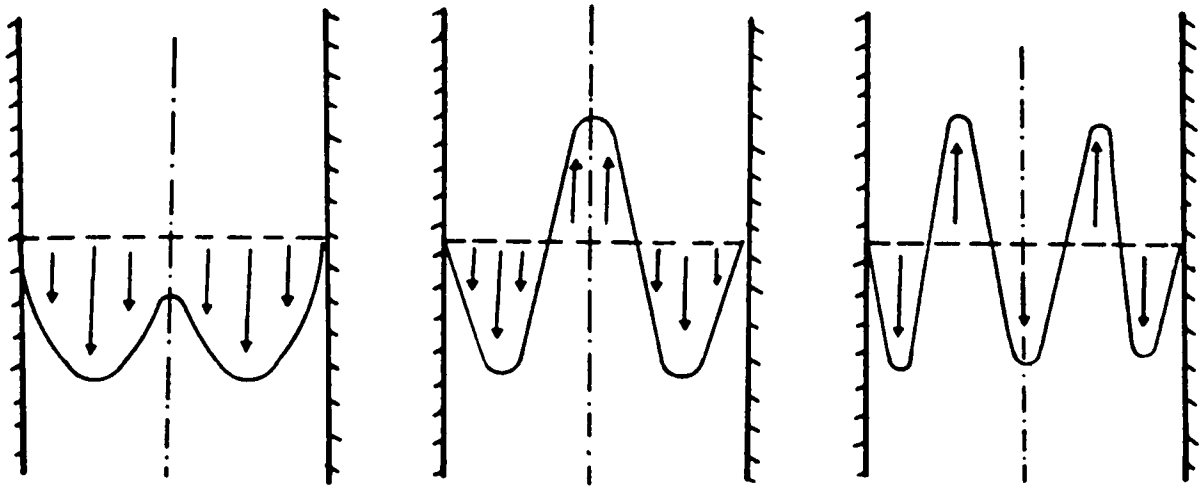

Figure 12. Flow reversal observed by Nuttal for swirling flow in a circular pipe [81].

5.3.2.1 Swirl Flow in a Pipe Expansion

This is the basic form of the dump combustor geometry. With the introduction of swirl, a central recirculation zone (CTRZ) is formed, in addition to the corner recirculation zone (CRZ) [74]. The recirculation zones are important in the design because most combustion occurs in

and near these regions. The nonswirling pipe expansion has only the CRZ and with the swirl imparted at the inlet, a central recirculation region appears and the size of CRZ decreases. The corner recirculation zone is reduced in the axial extent until it disappears for a swirl vane angle of 70 deg (Fig. 13). These predictions were obtained using the TEACH code with k-ϵ turbulence model. Novick et al. [84,85] obtained useful flow predictions for actual combustor geometries. One example is shown in Figure 14. With no swirl the CRZ fills the outer cavity. As swirl is introduced a CTRZ appears in conjunction with a decrease in the size of CRZ (see Fig. 14 for 45 deg swirl angle). Further increase in swirl angle results in continued enlargement of the CTRZ and a decrease in the size of the CRZ. At 75 deg the CRZ disappears. No direct comparison with experiments has been made.

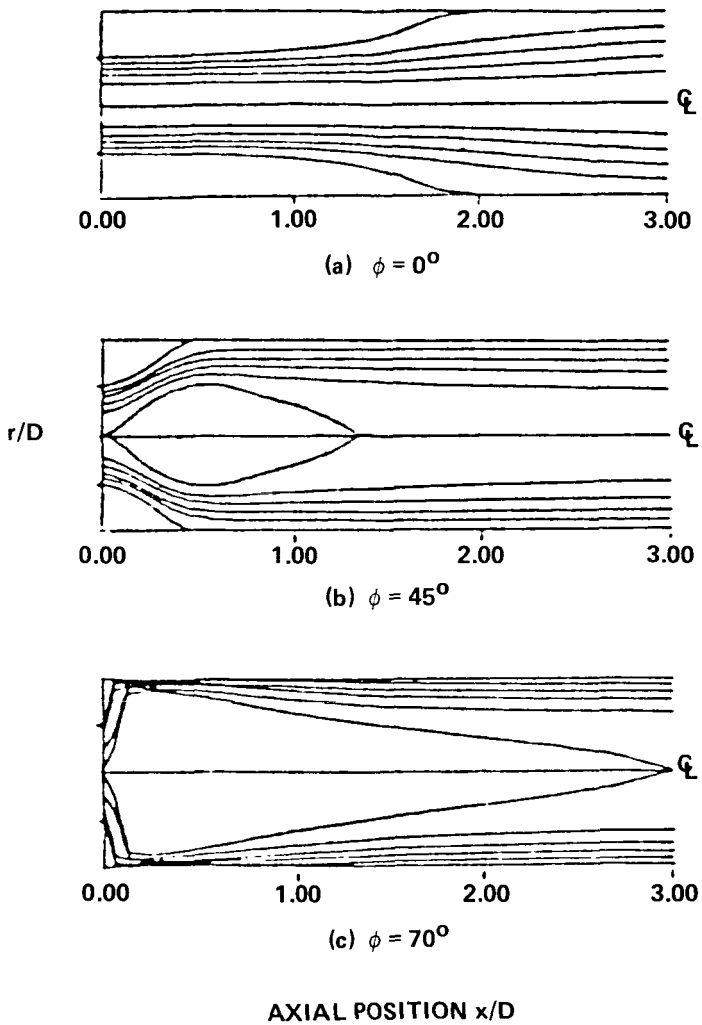

Figure 13. Predicted streamline plots with wall expansion angle α = 90 deg and various swirl vane angles ϕ. [74].

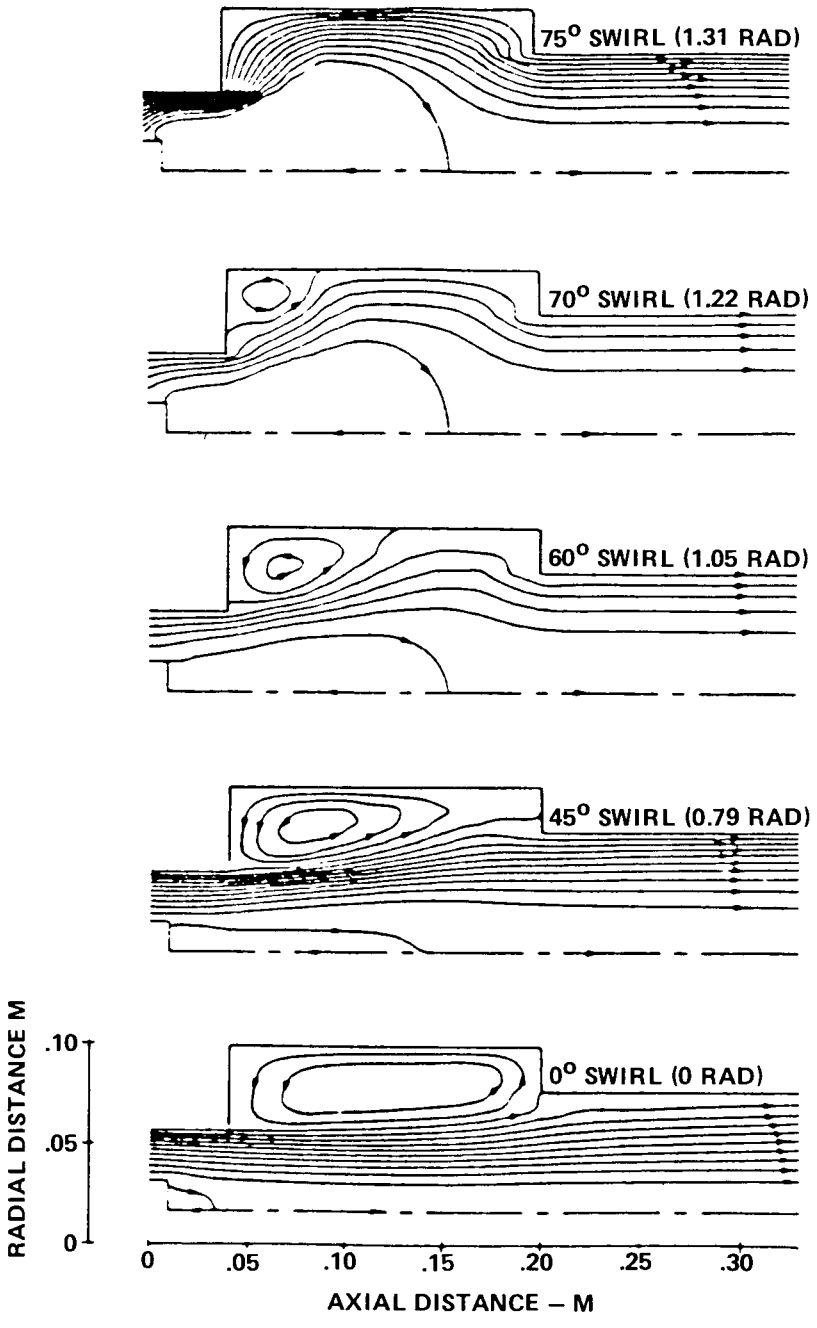

Figure 14. Effect of swirl vane angle on isothermal axisymmetric combustor flow field [84].

5.3.2.2 Confined Coaxial Jets

This basic configuration is being studied extensively both experimentally and theoretically because of its importance in combustor designs. Efforts have been made to predict the flow patterns for a range of swirl numbers. At low swirl numbers $S < 0.5$, there is only the corner recirculation zone. For swirl numbers $S \geqslant 0.5$ an additional central recirculation zone is observed. The swirl number is defined as

$$S = \frac{\int_0^R \rho \, Ur^2 \, W \, dr}{R \int_0^R \rho \, (U^2 - 0.5 \, W^2) \, r \, dr}$$

(S_o is the swirl number of the outer jet, S_i is the swirl number of the inner jet, and α is the velocity ratio of annulus to pipe).

Table 3 summarizes the recent numerical studies on swirling jets. As it is obvious from the table, all the studies use the k-ϵ turbulence model. Detailed analysis of the predictions of the k-ϵ model for swirling jet is presented by Habib and Whitelaw [72]. The recirculation length is underpredicted by about 20 percent for $\alpha = 1$. With increase in α, the prediction gets worse. This is attributed to the incorrect representation of the diffusion process in the k-ϵ model. For the flow with swirl, the model is incapable of predicting the velocity minimum obtained at the axis in the experiments. Figure 15 shows the velocity profiles for swirl and no swirl cases. This velocity minimum on the central line has not been predicted correctly in any of the studies reported. They also observe that the intermediate swirl number of 0.23 provides the flow which is more difficult to present by calculation methods since the near recirculation region is located away from the solid surfaces. With no swirl there is only the CRZ. With the swirl number of 0.5, the CTRZ is tied to the exit geometry and the downstream flow is easily represented. Srinivasan and Mongia [41] modified the k-ϵ model to include the Richardson number dependence through the constant C_2 of the model. They use the gradient Richardson number, and divide this into two: swirl Richardson number and curvature Richardson number quite arbitrarily. However, they find that at high swirl numbers, the curvature Richardson number has no influence on the flow but swirl Richardson number is the controlling one. They could not obtain convergent results for coswirl case. They modified their program to include radial pressure variations, which enabled them to obtain coswirl solutions. Coswirl solutions showed a central recirculation zone not observed in experiments. Ramos [86] claims that with the use of suitable initial condition, the standard k-ϵ model predicts the coswirl flow. His claim is not substantiated by providing the exact initial condition used and the justification for the conditions used. Hence, it is not of much use in understanding the prediction method. Novick et al [84,85] study several variations of the combustor configurations. They characterize the size and shape of the recirculation zones with swirl number, expansion ratio and the geometry. These results help one to get some idea of the predictive capability of the k-ϵ turbulence model for these configurations.

In general, in the prediction of confined vortex flows, the k-ϵ model performs rather poorly [88]. Figure 16 shows the predicted and measured tangential velocity profile in a vortex tube. It is seen that the standard k-ϵ model does not even predict the qualitative features of the flow while the ASM predictions agree well with experimental results [89]. Dixon et al. [90] employed the k-ϵ model for predicting the swirled coaxial jets and found that the model underpredicted the extent of the central recirculation region by about 20 percent. They also found that the prediction of the maximum recirculated mass

TABLE 3. CONFINED COAXIAL JETS

Reference	Flow Parameters	Turbulence Model	Properties Predicted	Remarks
Habib and Whitelaw [72]	Velocity ratio of annulus to pipe, α = 1,3; swirl No. S_o = 0, 0.23	k-ϵ	$\overline{U}$, k, $\overline{u_1^2}$, $\overline{w_1^2}$	• k-ϵ model unable to predict the velocity minimum at the axis. • Underpredicts the separation length. • Prediction becomes poorer as the velocity ratio increases.
Ramos [86]	α = 0.68, 0.69, 0.70, 0.74 S_o = -0.38, -0.19, 0, 0.21, 0.42 S_i = 0.59, 0.63, 0.68, 0.69, 0.71	k-ϵ	$\overline{U}$, $\overline{W}$	• predicts a recirculation zone for coswirl-not observed in experiments.
Novick et al. [84]	S_o = 0.67, 1.16, 1.83, 2.4	k-ϵ	$\overline{U}$, $\overline{W}$, Central line decay, stream line pattern	Radial profiles compare favorably with experiments. Qualitative agreements of separation zones CRZ and CTRZ.
Novick et al. [85]	• Expansion ratio • Swirler dimension • Double concentric reverse swirlers • Constricted exit	k-ϵ	Recirculation zones and flow patterns	Recirculation zones predicted well. The presence of reaction reduces CTRZ.
Srinvasan and Mongia [41]	• S_i = 0.577, S_o = 0.536 • S_i = 0.49, S_o = 0.507	k-ϵ k-ϵ modified. Modified program for pr. gdts.	$\overline{U}$, $\overline{W}$ flow patterns.	• k-ϵ predictions are no good. • Modified k-ϵ predicts the counter swirl well. • Could not produce coswirl solutions. • Accounting for pressure gradients results converged solution for coswirl. • Coswirl shows recirculation zone.
Sturgess et al. [87]	Coswirl and counter-swirl as in [41]	k-ϵ	$\overline{U}$, recirculation zones	Predicted solutions are very sensitive to the inlet boundary conditions.

flow rate in the central recirculation zone was still worse; it was half that of the measured one. Thus, the use of the standard k-ϵ model to highly swirling flows may not produce reliable results [91] and the use of ASM should be recommended.

The accuracy of the numerical schemes in predicting the swirl flows and the effect of inlet boundary conditions are briefly discussed in Section VI.

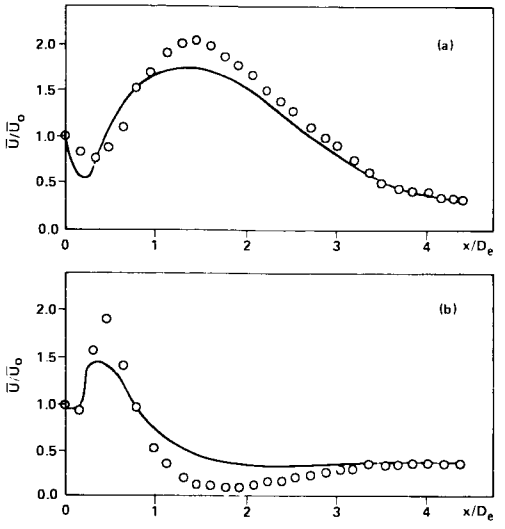

Figure 15. Measured and calculated distributions of the mean velocity. o Measurements, – calculations. (a) S = 0.0. (b) S = 0.23 [72].

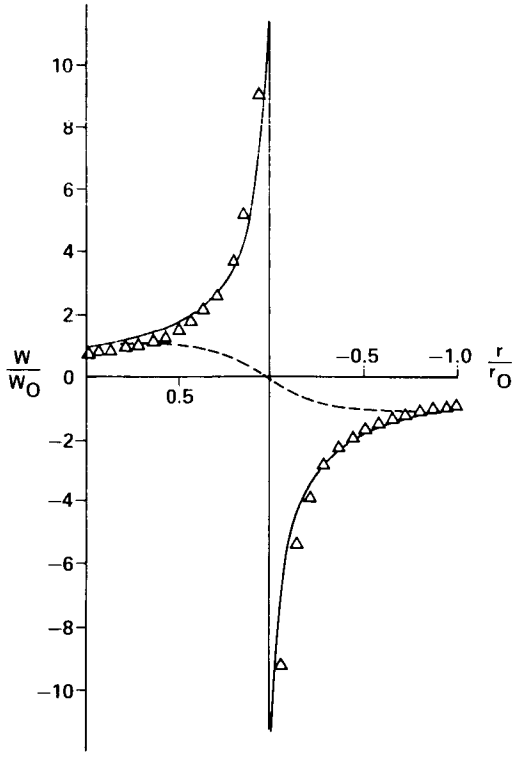

Figure 16. Predicted and experimental tangential velocity profiles in the vortex tube. – ASM, - - -k-ϵ model, $\triangle$ experimental. [89]

5.4 Three-Dimensional Computations

5.4.1 Noncircular Duct Flows

Turbulent flow in noncircular ducts is characterized by the everpresent secondary motions. The magnitude of the secondary motion depends on the geometry and is strongly influenced by the curvature. Presence of secondary flows makes the problem more difficult. One has to solve for the three components of velocity and additional equations for Reynolds stresses. To make the problem tractable, most studies on noncircular passages concentrate on fully-developed flow in uniform cross-section. (Developing flow was a test problem in the 1981-Stanford conference and will be presented in this section.)

The cause of secondary motion has been investigated and explained. Recently, Speziale [92] has proven mathematically that the secondary flows in noncircular ducts result from a nonzero difference in the normal Reynolds stresses on planes perpendicular to the axial flow direction. He also shows that the widely used k-ϵ turbulence model has no built-in mechanism for the development of secondary flow, while the second order closure models do.

Launder and Ying [93] were the first to carry out a detailed numerical prediction of the turbulent flow in a square duct. They employed the simplified form of the Reynolds stress model of Hanjalic and Launder [94] which advocates the solution of seven coupled nonlinear differential equations in addition to those of mean flow quantities (Section 3.3). Launder and Ying found that for fully developed flows the convection and diffusion terms in the stress transport equations may be neglected. This important simplification results in the removal of all differential coefficients of $\overline{u_i u_j}$ and hence algebraic in the latter (the reasoning putforth in ASM, Section 3.5). They obtain the following form of equations:

$$\overline{u_1^2} - \overline{u_2^2} = -C\,l^2\left[\left(\frac{\partial U_3}{\partial x_1}\right)^2 - \left(\frac{\partial U_3}{\partial x_2}\right)^2\right]$$

$$\overline{u_1 u_2} = -C\,l^2\left(\frac{\partial U_3}{\partial x_1}\right)\left(\frac{\partial U_3}{\partial x_2}\right) \qquad (49)$$

They solve the kinetic energy equation in addition to the three momentum equations and use the algebraic relations for the stresses (49) and the length scale.

Later investigations employed a differential equation for ϵ. This method of solving five differential and algebraic equations for the stresses has been successfully employed for solving the flow in rectangular, triangular and elliptic ducts, and tube assemblies by Gosman and Rapley [95]. They use a boundary fitted (orthogonal curvilinear) coordinate system for the noncircular ducts. Comparison of the ASM equations with laminar contributions reveals that axial stresses $\overline{u_1 u_3}$ and $\overline{u_2 u_3}$ depend on turbulent viscosity and axial strain rate in a Newtonian fashion; but the cross-planar stress equations are distinctly different from the Newtonian relations depending on the axial as opposed to cross-planar strain rates. It is this feature, as explained by Speziale, that is responsible for the turbulence-driven secondary motion.

Perhaps, the most exhaustive study of fully-developed turbulent flow in noncircular ducts is that of Gosman and Rapley [95]. They studied the flow in square, rectangular, triangular, and elliptic ducts and tube assembly passages and compared the accuracies of the predictions by different turbulence

models. Detailed comparison of the mean velocity, secondary velocities, friction factor and Reynolds stress components with those of experiments [96] and other numerical predictions were presented for the square duct. They compared the prediction of the algebraic stress model, Reynolds stress model [97], and modified Reynolds stress model [98]. The modification in Noat et al. [98] is only the finite difference method of solution. By employing a local block inversion method, they solved the flow and stress equations simultaneously rather than sequentially as in other methods. Figures 17 and 18 show the comparison of the prediction by the three models with the experiment [99]. The three models predict the axial (Fig. 17) and secondary velocities (Fig. 18) equally well. However, the Reynolds stress components (Fig. 19) are not predicted well. This may be partly due to the expected underprediction of the normal stress anisotropy, with the set of constants used.

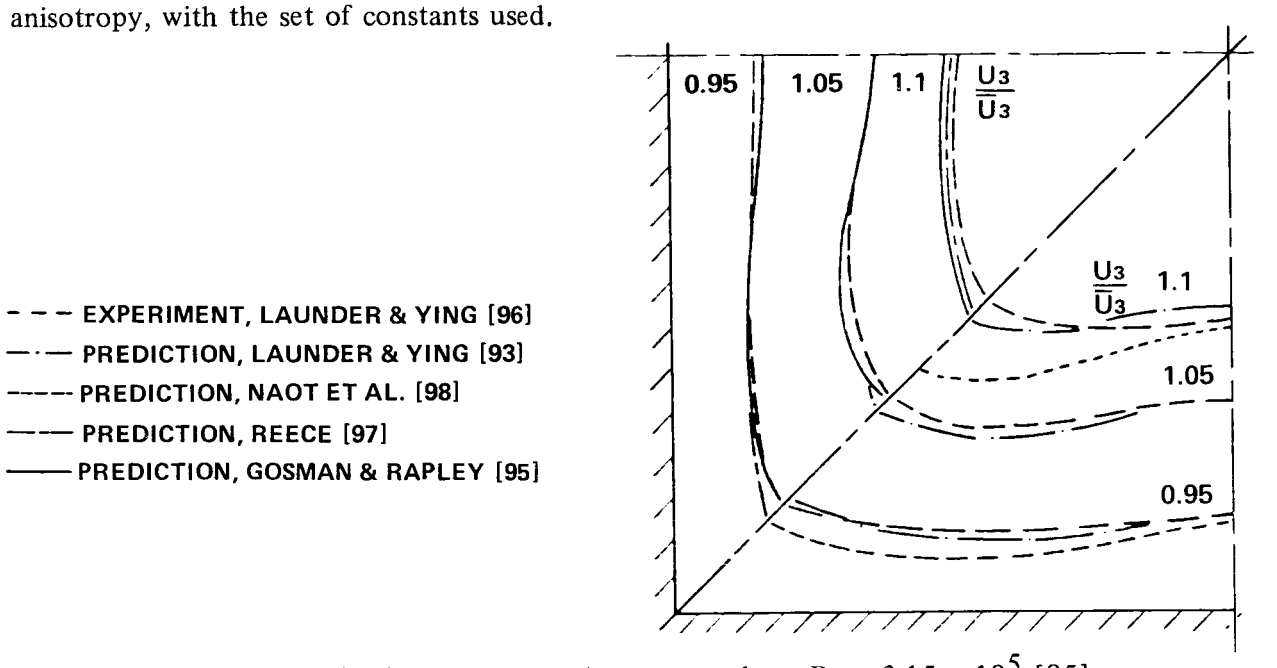

Figure 17. Axial velocity contours in a square duct, Re = 2.15 x 10^5 [95].

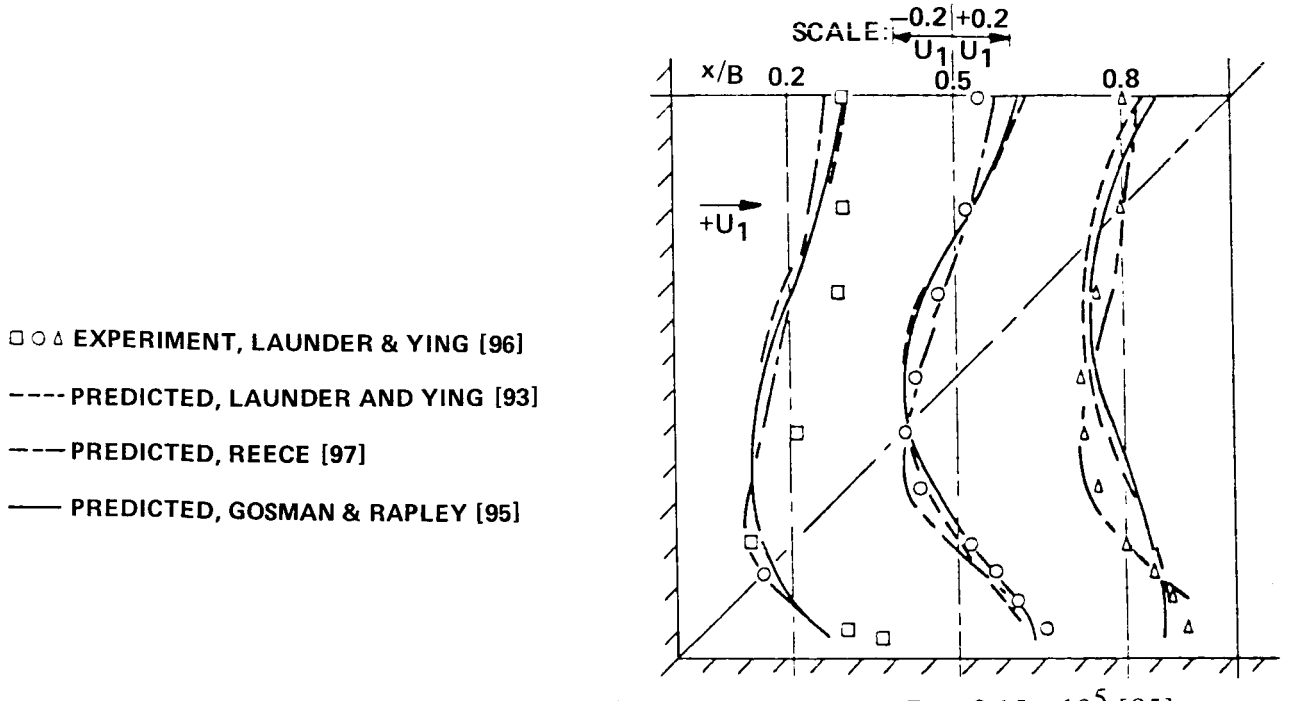

Figure 18. Secondary velocity profiles (U_1/U_3*) in a square duct, Re = 2.15 x 10^5 [95].

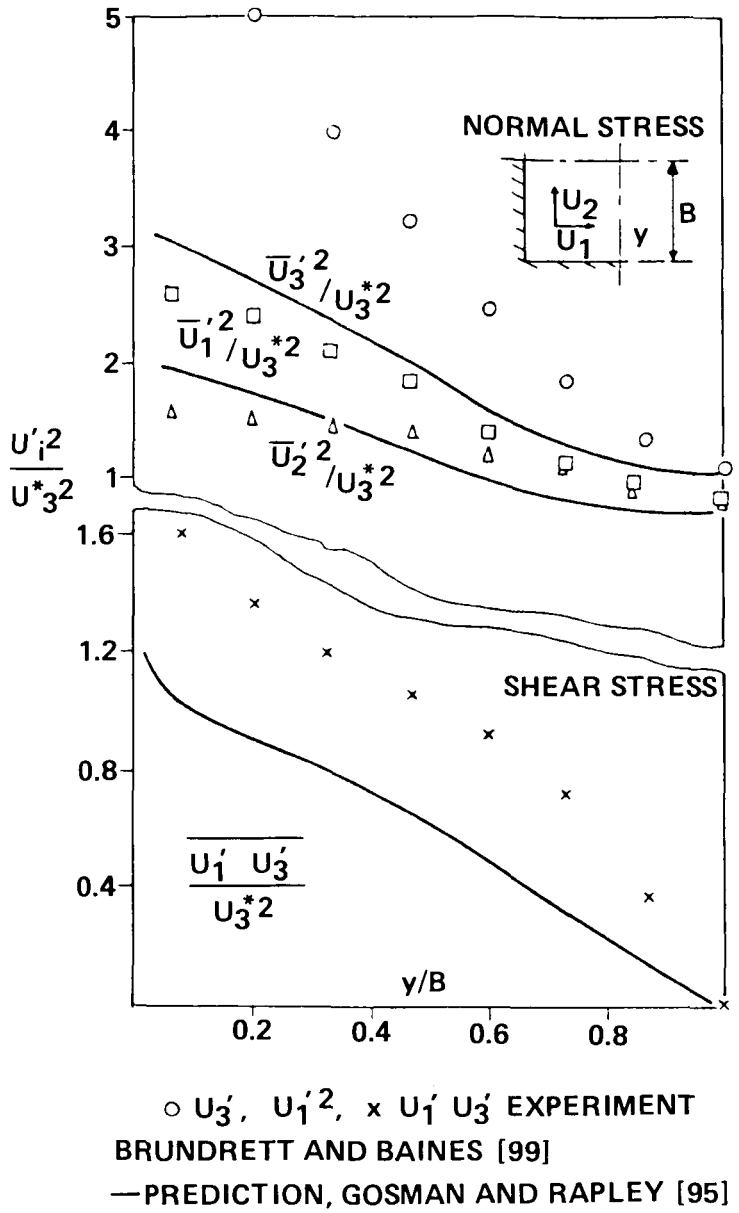

Figure 19. Reynolds stress profiles in a square duct, Re = 8.3 x 10^4 [95].

5.4.2 Developing Flow in a Square Duct

This was a test problem at the 1981-Stanford conference on complex turbulent flows. Only three groups attempted this problem. Table 4 shows the models used by them and comments on the predicted results. All three groups use the ASM-based method. References 46 and 100 use a differential equation for ϵ, while Reference 101 uses an algebraic equation. As indicated in the table, the model predictions are very poor. This means that the algebraic stress model is not good for developing flow where local equilibrium assumption is not valid. Perhaps only the Reynolds stress model is capable of predicting the developing flow in a square duct.

TABLE 4. DEVELOPING FLOW IN A SQUARE DUCT

Reference	Turbulence Model	Computed Flow Quantities	Remarks
Rodi et al. [46]	ASM with differential equation for ϵ	Mean axial velocity, secondary flow velocities.	• Secondary velocities overpredicted by a factor of 2. • Streamwise velocity poorly predicted along the diagonal. • Gradients of secondary velocities were strong (in ASM). If these terms were omitted, calculation becomes unstable.
Nakayama et al. [100]	ASM with differential equation for ϵ	Mean axial velocity, secondary flow velocities, pressure drop.	• Distortion of the wall shear profile over the peripheri overpredicted. • The centerline velocity peak is predicted to be about 7 hydraulic diameters upstream compared to experiments. • Underpredicts secondary flow velocity along the diagonal. • Pressure drop fairly well predicted.
Coustiex et al. [101]	ASM with algebraic equation for ϵ	Mean axial velocity, secondary flow velocities.	• Poor prediction of secondary flow velocities.

VI. NUMERICAL METHODS

The prediction methods use various numerical schemes and solution procedures whose performance in different regions of the same flow and in different flow situations are not well established. Two related problems which influence the predicted solutions are briefly discussed below.

6.1 False Diffusion

Most methods employ an upwind difference scheme which is known to introduce false diffusion errors. The false diffusion coefficient at any computational cell can be computed from the formula [102,103]

$$\Gamma_f = \frac{\rho\, U\, \Delta x \Delta y \sin 2\theta}{4\,(\Delta y \sin^3 \theta + \Delta x \cos^3 \theta)} \tag{50}$$

where Δx and Δy are the cell dimensions and θ is the angle made by the resultant velocity at the grid lines. Figure 20 shows, for a hybrid central-upwind scheme with a fine grid (42 x 42) which produces a mesh independent solution, the variation of maximum normalized false diffusion coefficient along the duct of backstep flow (Section 5.1). The false diffusion coefficient shown is the value normalized with local value of turbulent viscosity and multiplied by the ratio of the local-to-maximum shear stress at any station [56]. The maximum value of the factor is about 0.2 and the estimated error caused by this false diffusion in the prediction of the reattachment length is about 0.3H. For example Syed et al. [53], by using an accurate scheme (bounded Skewed Upwind Scheme), obtain an increase of 0.35H in x_R over hybrid scheme, for a fine mesh. In the presence of numerical diffusion in the recirculation region, no meaningful comparison of two turbulence models can be made. On a moderate grid, upwind differencing scheme may be insensitive to changes in turbulent viscosity. If one is unable to accommodate a fine enough mesh, then the alternative is to use a higher order accurate scheme. McGuirk et al. [104] use a selective mesh refinement procedure which reduces the number of mesh points required but maintaining a higher accuracy. They identify the regions of "false diffusion" present in the solution, with a given grid, by estimating the magnitude of the local truncation error in the converged solution of the discretized equations. This identifies the local regions where the Peclet number is high. They change the difference scheme depending on the value of the Peclet number: if $|Pe| < 2$, they use central differencing scheme and if $|Pe| > 2$, they use upwind difference scheme. This guarantees numerical stability and produces accurate results. This procedure may be useful in comparing two different turbulence models. But, it is too involved and expensive to use as a general solution procedure.

Numerical differencing schemes that reduce the false diffusion have been developed [105,106]. Leschziner and Rodi [37] evaluated the performance of three difference schemes – hybrid central/upwind differencing scheme (CUDS), hybrid central/skewed-upwind differencing scheme (CSUDS), and quadratic upwind weighted differencing scheme (QUDS) – on annular and twin parallel jet flows and found that the later two (CSUDS and QUDS) reduce the false diffusion errors significantly. Syed and Chiappetta [53] have tested several schemes for accuracy in predicting the swirl flows. They found that the bounded skewed upwind scheme (BSUDS) produced more accurate results than the hybrid (CUDS) scheme.

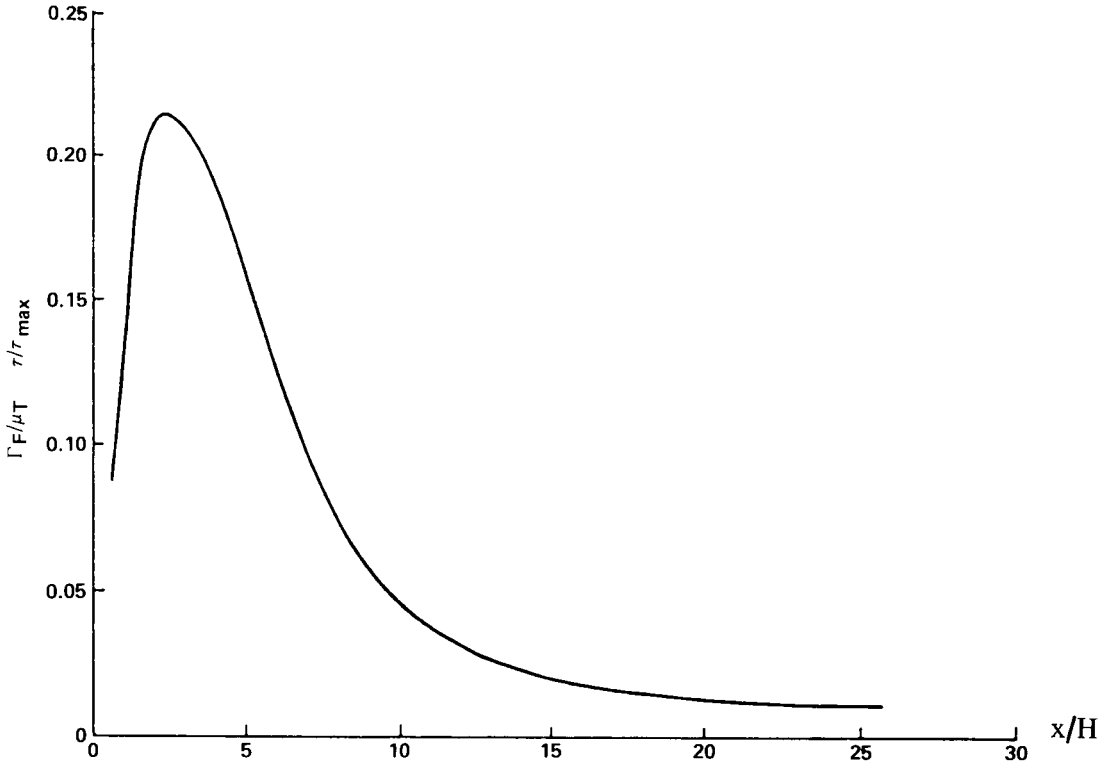

Figure 20. Maximum relative level of false diffusion coefficient at any section [56].

6.2 Inlet Boundary Conditions

Inlet conditions are usually considered of minor importance while evaluating the performance of turbulence models against experimental data. Assumed boundary conditions can lead to wrong conclusions about the performance of the model. In particular, the inlet profiles of k and ϵ can have a significant effect on the flow downstream. The profiles of k may be estimated from the experimental results. But no satisfactory method of evaluating inlet ϵ profile is available. In the flow over a backward step, for example, if one starts with a larger initial length scale (larger viscosities), the prediction is expected to give a shorter reattachment length. But the predictions do not show such a trend.

The inlet conditions become more "controlling" when the inlet flow has a swirl component. Sturgess et al. [87] studied in detail the effect of inlet boundary conditions in swirl flows. They found that the computations were sensitive to the inlet conditions, and might affect the solution in the entire flow domain. Many times, by manipulating the inlet profiles, a better fit to the experimental data can be obtained. For example, Ramos [86] claims that k-ϵ model predicts a recirculation zone for both co- and counter-swirl conditions, if suitable initial conditions are used. Leschziner and Rodi [107] find that the inlet conditions for k and ϵ play as crucial a role in achieving predictive accuracy as turbulence modeling details. Thus, in the absence of experimental inlet profile data, careful and "judicious" choice of the initial condition estimation is essential for a physically meaningful prediction.

Typical Inlet Conditions Employed in Predictions

	k_{in}	ϵ_{in}
(a) Flows Without Swirl		
Qin [62]	$0.003 \times U_{in}^2$	$0.09 \times k_{in}^{3/2}/(0.03 \times D/2)$
(b) Flows With Swirl		
Habib and Whitelaw [72]	$k = 1/2\ [u'^2 + v'^2 + w'^2]$ u' – experiment $v' = w' = 0.6\ u$	$0.09 \times k_{in}^{3/2}\ (0.03 \times R)$ (R is the radius of pipe or annulus)

Sturgess et al. [87] studied the effect of inlet boundary conditions on the prediction of swirl flows. They found that the numerical solutions were very sensitive to the inlet boundary conditions and the overall accuracy of the prediction depended on the grid system. Syed and Sturgess [108] describe the present status of the predictive capability for the swirling recirculating nonreactive flows (Fig. 21). To this should be added the inability to predict the coswirl flow, the central line minimum, and the radial variations of the mean velocity as discussed in Section 5.2.3. Detailed experimental data for coaxial jets with and without swirl can be found in References 109 and 110, for evaluating turbulence model predictions.

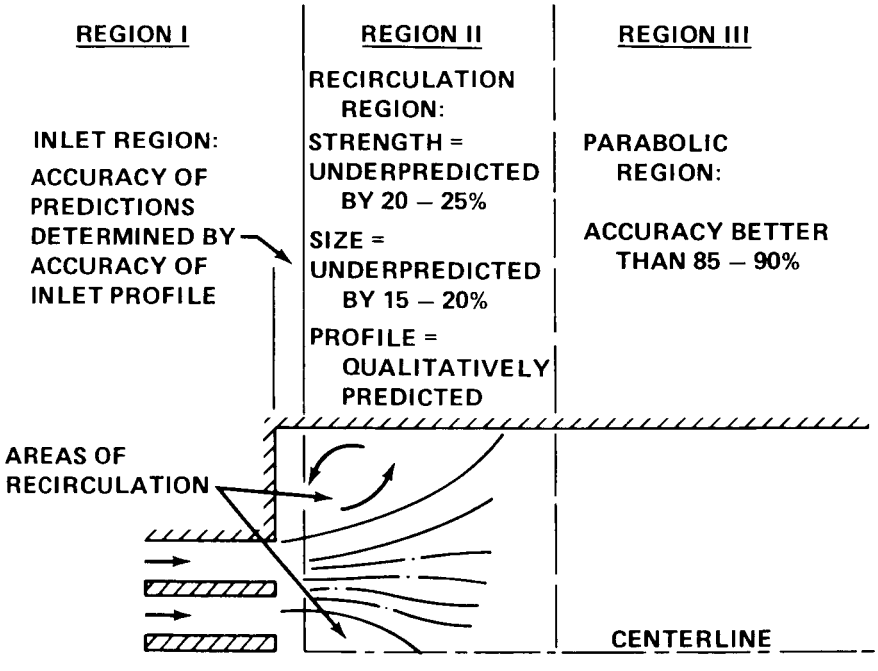

Figure 21. Summary of the accuracy of predictions in the various regions of flow with swirl [108].

VII. COUNTERGRADIENT TRANSPORT AND TURBULENCE MODELING

The eddy viscosity type models assume that the gradient transport hypothesis holds in all the regions of the flow. However, it is known that small regions of countergradient transport or negative turbulent energy production exist in many flow situations such as asymmetric channel flow, wall jets, wake flows, perturbed shear layers, etc. Beguier et al. [111] discuss a variety of flow situations which contain regions where the product $-\overline{uv}\ \partial U/\partial y$ becomes negative. Townsend [112] was the first to recognize and explain the small region of countergradient transport of momentum in a plane wake. In this region, transport of momentum consists of two parts: (a) gradient type diffusion by small scales and (b) convection by large scale motions of eddies comparable in size to the characteristic length scale of the problem. Hinze [113] extended this concept to asymmetric flow. To account for the contribution due to the bulk transport by the large eddy, one adds a second term in the expression for Reynolds stress (see, for example Ref. 3, page 372). The additional term is proportional to either $\partial(\overline{v^2})^{1/2}/\partial y$ or to $\partial(\overline{q^2})^{1/2}/\partial y$ where $(\overline{q^2})/2$ is the kinetic energy.

Beguir et al. [111] analyzed different flow situations in which such regions of countergradient transport occurs. They find that a direct relationship between the sign of the gradient of $(q^2)^{1/2}$ and the displacement, e, of the minimum exists. The displacement e is defined as

$$e = y_{(\overline{uv}=0)} - y_{(\partial U/\partial y=0)} = \frac{C}{\nu_t} l_o^3 \frac{\partial}{\partial y} (\overline{q^2})^{1/2} \tag{51}$$

where C is a constant (= 0.1), l_o is a characteristic length scale, such as the width of the channel. The product $e \cdot \partial(\overline{q^2})^{1/2}/\partial y$ was negative for the majority of the flows considered, where the flow asymmetry or the perturbation was small. However, when the asymmetry, such as the interaction of wake behind cylinders of unequal diameters, or the perturbation was strong, the product was positive. Their flow visualization of the interacting wake behind the cylinders showed that in that case, merger (or pairing) of the vortices of the same sense of rotation occurred, similar to that found in shear layers [114,115]. This suggests that the small asymmetry or perturbation results only in a change in the orientation of the generally elliptic vortex structure (against the gradient $\partial U/\partial y$ instead of along the gradient) and results in only minor changes in turbulence quantities. This results in a negative sign of the product $e \cdot \partial(\overline{q^2})^{1/2}/\partial y$. The strongly asymmetric or perturbed flow condition results in merger of large scale eddies, in which case the variation in turbulence quantities is too complex. This situation cannot possibly be described by simply adding a term to the Reynolds stress equation. An example of the changes in turbulence quantities in a perturbed axisymmetric mixing layer [116] is shown in Figure 22. It can be seen that for the strong perturbation, in which localized vortex merger occurs, the shapes of the Reynolds stress and the longitudinal velocity fluctuation profiles are different from those of unperturbed or of small perturbation and are too complex. Oster and Wygnanski [117] present a detailed study of the variations of the turbulence quantities in a perturbed plane mixing layer. Employing Reynolds stress model one can predict the small asymmetric or perturbation case satisfactorily [23] or even by a simplified form of the Reynolds stress model [94]. However, it is not known if the Reynolds stress model can predict the strongly asymmetric or perturbed case.

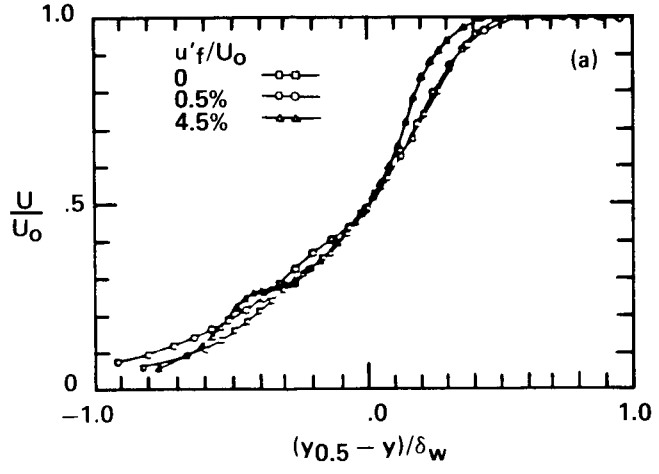

(a) Mean velocity profiles.

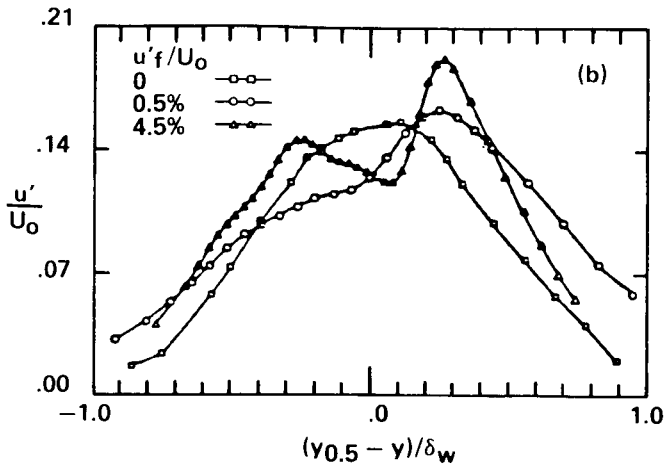

(b) Longitudinal velocity fluctuations.

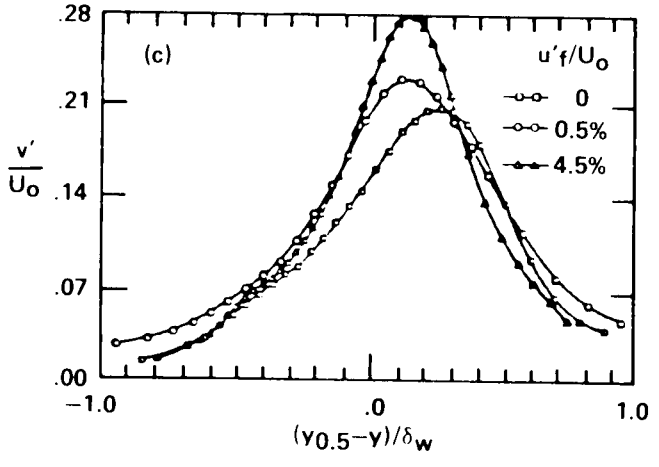

(c) Transverse velocity fluctuations.

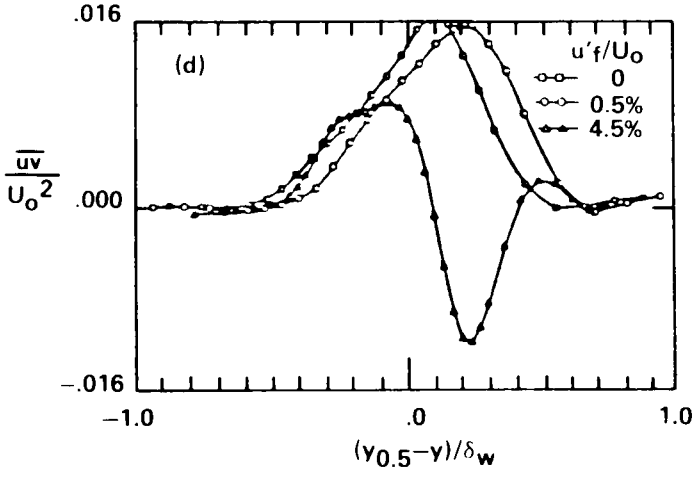

(d) Reynolds stress profiles.

Figure 22. Perturbed mixing layer characteristics [116].

For the transport of any scalar quantity, ϕ in a turbulent flow, one can define an equation similar to that of (51).

$$e_\phi = y_{\overline{\phi v}=0} - y_{(\partial\phi/\partial y=0)} = \frac{C_\phi}{\nu_t} l_\phi^3 \frac{\partial(\overline{q^2})^{1/2}}{\partial y} \quad . \tag{52}$$

Beguier et al. [111] considered this for the case of asymmetric mean temperature (θ) profile. Again for small perturbations the product $e_\theta \cdot \partial(\overline{q^2})^{1/2}/\partial y$ was negative and for a strong interaction case it was positive.

The countergradient diffusion in flows involving combustion has been studied by Libby and his co-workers [118,119]. They avoid the gradient transport assumption and develop a second order closure model. They attribute this diffusion to the differential effect of the mean pressure gradient on cold reactants and hot products. Jones and Whitelaw [83] also observe that the countergradient diffusion is due to the preferential influence of the mean pressure gradient on low- and high-density gases which manifest through the terms like $\overline{\rho' u_j''}\ \partial\bar{p}/\partial x_i$ and $\overline{\rho' \phi''}\ \partial\bar{p}/\partial x_i$ in the exact Favre-averaged (density weighted) [120] Reynolds stress and turbulent scalar flux transport equations.

Spalding [121] calls the countergradient diffusion as "pressure gradient" diffusion, because of its connection to the pressure gradient. He observes that the turbulence modelers have been concerned exclusively with Kelvin-Helmholtz (shear generated vortex roll-up and pairing) instability and little attention has been given to Rayleigh-Taylor instability. His two-fluid model takes care of the later and is expected to describe the so-called countergradient or pressure gradient diffusion process. However, it is not clear at this point, if it can describe the shear generated variations of turbulence quantities in small and strongly perturbed/asymmetric flow discussed above, as well.

VIII. COMPUTATIONS OF RECIRCULATING FLOWS WITH PHOENICS CODE

PHOENICS is a general purpose flow simulation code developed by Prof. Spalding and his associates at the Imperial College, London. The acronym PHOENICS stands for Parabolic Hyperbolic or Elliptic Numerical Integration Code Series. The code is now available commercially through the CHAM of North America in the U.S. and the CHAM of the United Kingdom in the U.K. The general features of the program are discussed by Spalding in Reference 122. The basic concepts and solution procedures employed in the code can be found in Reference 123. Here we present the computational results obtained with the k-ϵ model using the PHOENICS code for two flow configurations: (i) the flow over a backward facing step and (ii) the flow over a square obstacle in a two-dimensional channel. Only a brief discussion on the results is included. The sensitivity of the solution to the inlet boundary condition and the difference in the k-ϵ model predictions for the axisymmetric and asymmetric channel expansions will be discussed in a forthcoming report.

8.1 Flow Over a Backward Facing Step

This is the benchmark problem discussed in Section 5.1.1. The layout of the grid for the present computation is shown in Figure 23. The grid used is an adjusted (more grid lines near the walls) 42 x 42 grid to produce a grid independent solution. The expansion ratio is 1·5. The flow pattern with the recirculating region behind the step is shown in Figure 24. The length of the recirculation region x_R is equal to 5.8H, about the same as obtained in other k-ϵ model predictions. Depending on the ratio of the mesh sizes in the x and y directions ($\Delta x/\Delta y$), sometimes the solution exhibits a long tail for the recirculation region [62]. Figure 25 shows the contours of the kinetic energy in the flow domain. A large variation of the kinetic energy is observed in the separated shear layer and in the wall layer downstream of the step (the contours in the core region have very low levels of k as would be expected). The contours of ϵ, the dissipation rate of k, are shown in Figure 26. Here again contours in the core region have very low levels of ϵ. The maximum variation of ϵ occurs near the convex corner of the step. Figure 27 shows the static pressure contours in the flow field. As would be expected, the maximum static pressure variation occurs across the recirculating region. Thus, the predicted flow parameters show qualitative agreement with the experimental results. But, quantitatively, the prediction shows poor agreement with the measured ones both in the recirculating and redeveloping regions.

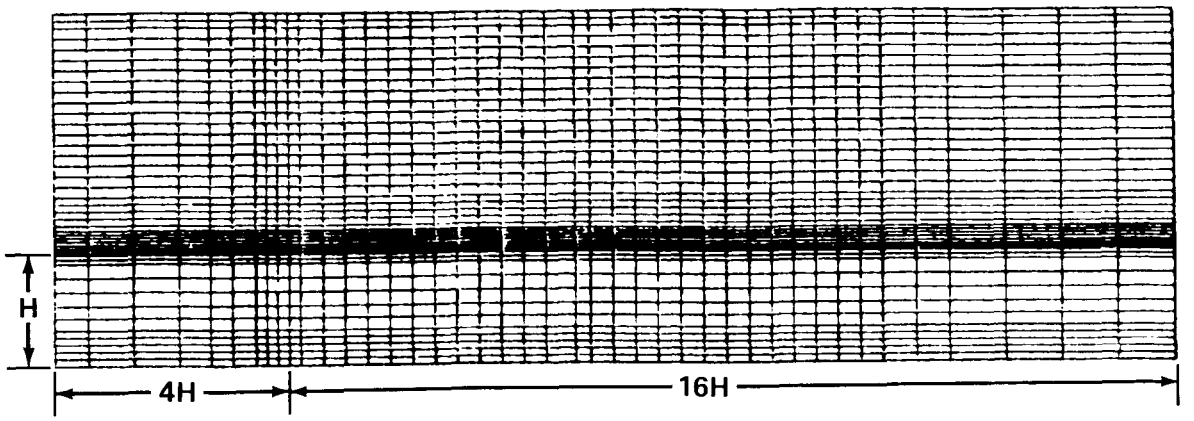

Figure 23. Calculation domain and grid layout for backward facing step.

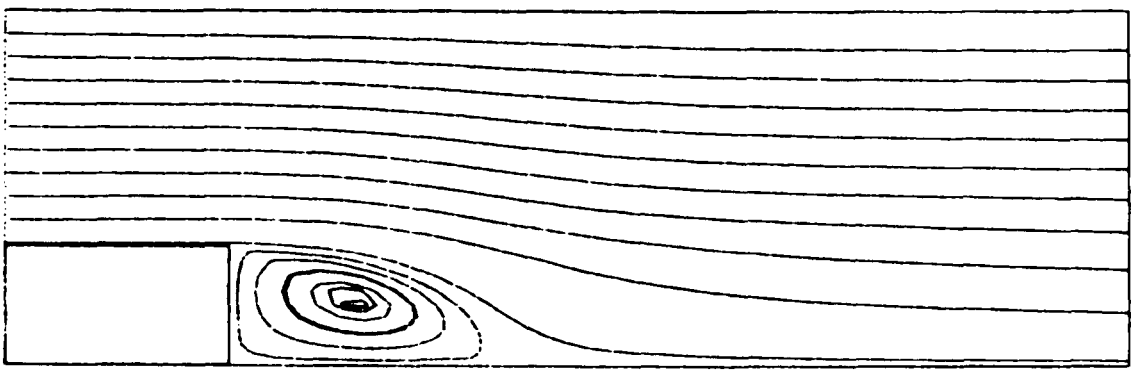

Figure 24. Streamline pattern.

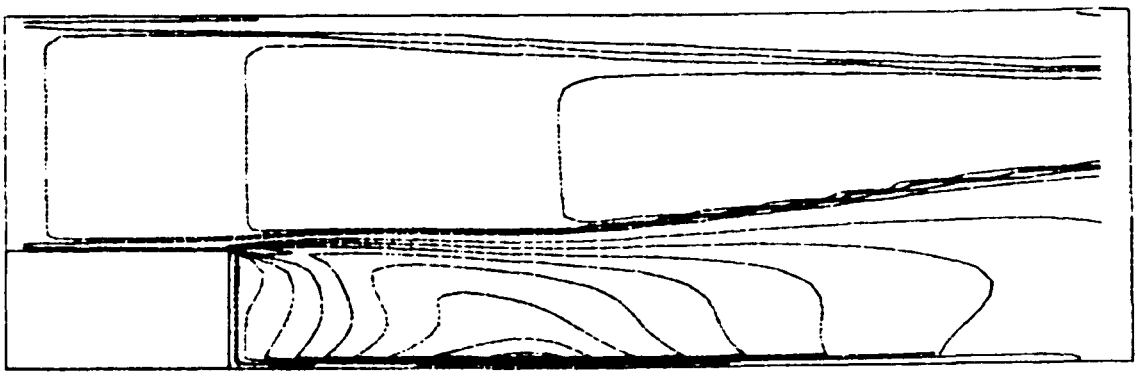

Figure 25. Kinetic energy contours.

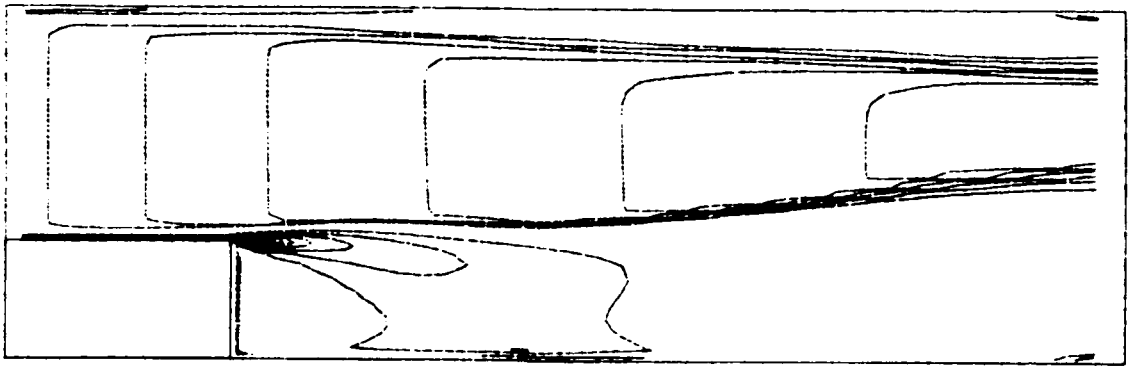

Figure 26. ϵ-contours.

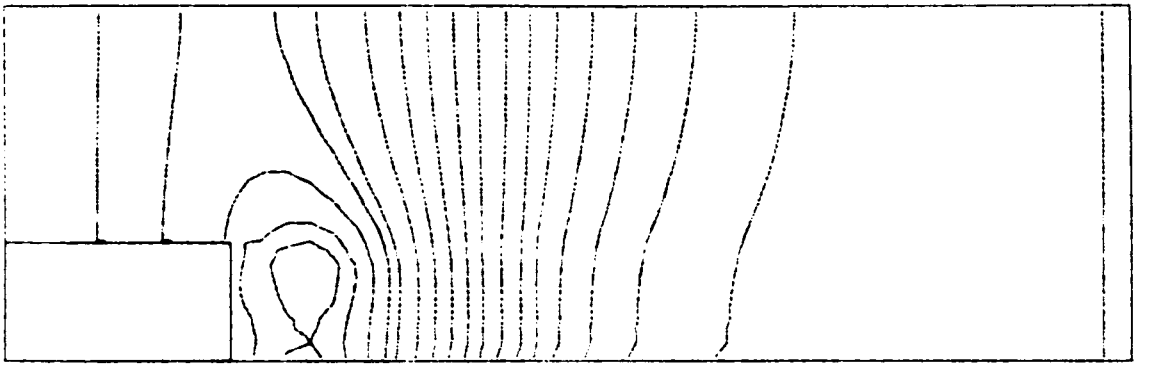

Figure 27. Static pressure contours.

8.2 Flow Over a Square Obstacle in a Two-Dimensional Channel

The flow geometry and the flow conditions are the same as in Reference 61 and discussed in Section 5.1.3. The grid layout for this problem is shown in Figure 28. The grid lines are uniformly spaced in the y-direction and adjusted in the x-direction. The grid employed is 40 x 47, which produces a nearly grid independent solution. There are four grid lines in the width of the obstacle. The flow pattern obtained is shown in Figure 29. The flow separates at the upstream corner of the obstacle and there appears to be a small recirculating region (indicated by the sharp turn of this streamline and the static pressure contours, Fig. 32) on the obstacle. Durst and Rastogi [61] found this separating streamline to reattach on the obstacle itself (Fig. 8). However, their experimental results show no reattachment on the obstacle. The length of the separated region is x_R = 6.6 H in the present prediction as compared to $\approx$ 7·5 H observed in the measurement. Considering the nature of the flow, this flow is slightly better predicted than the flow over a backward facing step. The reattachment length is underpredicted by only about 12 percent, while for the backstep flow x_R is underpredicted by about 20 percent. The kinetic energy contours are shown in Figure 30. Because of the accelerating and decelerating nature of the flow no core region (downstream of the obstacle) in which the contour levels are very low, is observed, as in the backstep flow. Figure 31 shows the contours of the dissipation rate ϵ in the computational domain.

The static pressure contours shown in Figure 32 indicate large variations of pressure in the recirculation region behind the obstruction and the region over the obstruction. Thus the qualitative features of the flow are in good agreement with experiments. Further aspects of the predictions of these flows will be reported in the forthcoming report.

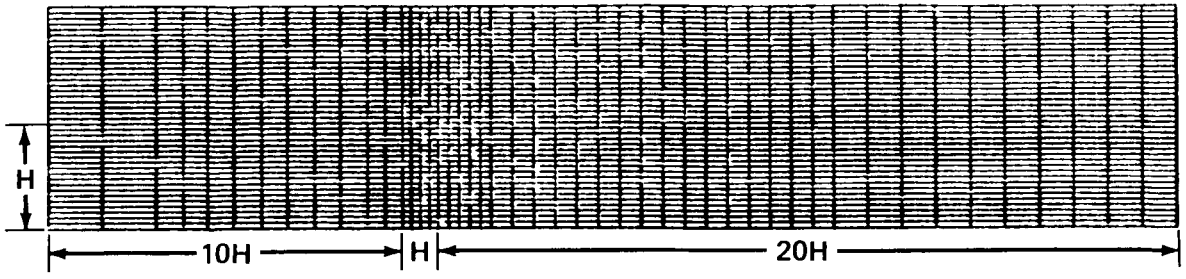

Figure 28. Calculation domain and grid layout for flow over a square obstacle.

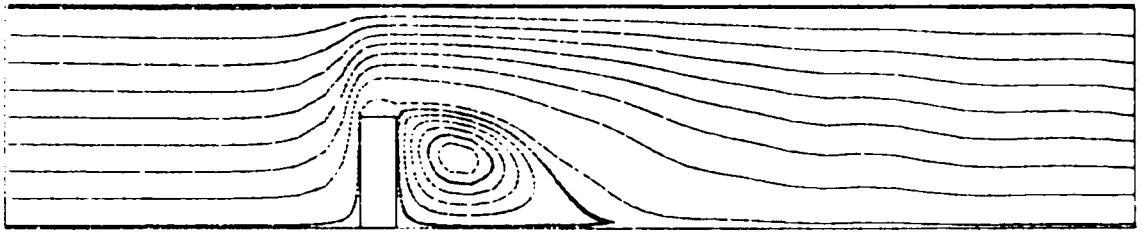

Figure 29. Streamline pattern.

Figure 30. Kinetic energy contours.

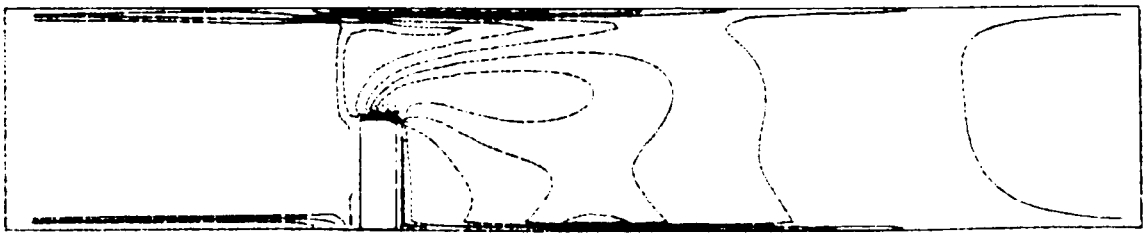

Figure 31. ϵ-contours.

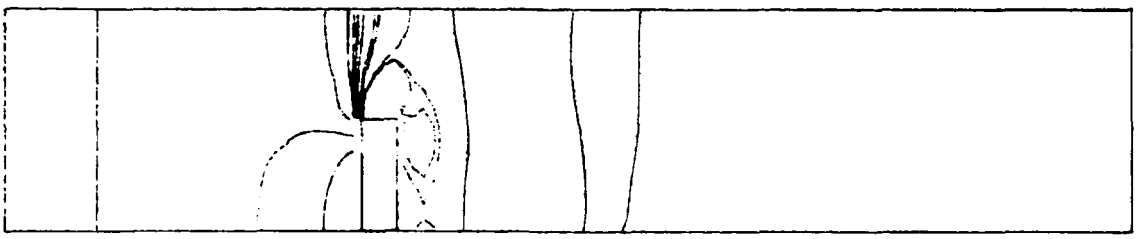

Figure 32. Static pressure contours.

IX. OTHER APPROACHES TO TURBULENT FLOW COMPUTATION

In this section, brief descriptions of three other approaches to turbulent flow computation, namely the vortex method, the large eddy simulation and the direct simulation are given. These methods are sometimes called higher level simulations, since they incorporate more flow physics than is possible with turbulence models. They are still more of a research tool than a scheme for engineering calculations. The computational memory and time requirements of these methods are typically high. Hence, the time for their implementation to aid the engineering flow analysis is yet to come.

9.1 Vortex Method

With the recognition of the existence of large-scale organized structures at least in the initial regions of mixing layers, jets and wakes, vortex method has received renewed emphasis in recent years. It has been used extensively to study the dynamics of large scale structures, since these large scale features arise from the properties of a rotational but inviscid flow. The idea is to represent turbulence as a superposition of interacting vortices. Saffman and Baker [124] provide an excellent account of vortex interaction studies. Leonard [125] reviews the concepts and methods of vortex flow simulation, including those for three-dimensional flows. Aref in his recent review [126] on the solution of two-dimensional Euler equations, discusses the use of vortex methods in the studies of transition to turbulence and the onset of chaos.

The widely used vortex method is the point vortex method. In this approach, the vorticity originally confined in a thin layer is concentrated further into a finite number of point vortices. In other words, the piecewise continuous distribution of vorticity ω is replaced by a sum of N δ functions.

$$\omega(\mathbf{X},t) = \sum_{n=1}^{N} \Gamma_n \, \delta[\mathbf{X}-\mathbf{X}_n(t)] \tag{53}$$

where δ is the Dirac delta function, $\mathbf{X}_n = (x_n, y_n)$ is the location of the nth vortex of circulation Γ_n. The motion of vortices is followed by integrating the system of ordinary differential equations

$$\frac{d\mathbf{X}_n}{dt} = U(\mathbf{X}_n,t) \quad . \tag{54}$$

The solution of equations (53) and (54) represents the solution of the two-dimensional Euler equations:

$$\frac{\partial \omega}{\partial t} + (U \cdot \nabla)\, \omega = 0 \quad , \tag{55}$$

$$\nabla^2 \psi = -\omega \quad , \tag{56}$$

$$U_x = \frac{\partial \psi}{\partial y} \quad , \qquad U_y = -\frac{\partial \psi}{\partial x} \quad . \tag{57}$$

No precise answer can be given for the question of the number N of the vortices required for a simulation. For a given N and t, confidence in the method is based on the requirement of the simulation and is often limited by the computer memory and time requirements.

Experimental studies on perturbed mixing layers and jets suggest that the sensitivity of the normally turbulent flows to external forcing is related to the rotational inviscid behavior of these flows. Hence, vortex methods have been used to study these perturbed flows. Acton [127] studied the characteristics of the "preferred mode" in circular jets. Vortex method has also been used to study the turbulence suppression in perturbed shear layers, and vortex roll-up, pairing, etc., in perturbed plane jet flows [128,129]. These studies depict clearly the dynamic features of the large scale vortical structures observed in the experiments. The vorticity and Reynolds stress contours during pairing of vortex structures in a perturbed mixing layer obtained using the vortex-in-cell method are shown in Figure 33. This corresponds to the orientation of pairing structures, for which a region of countergradient transport will result in the time mean field.

In Chorin's method for viscous flows [130], the inviscid outer flow is solved via discrete vortices and viscous effects are incorporated via random walks for each vortex. Recently Chorin and his coworkers have employed vortex methods for the study of turbulent combusting flows [131,132]. Beljaars et al. [133] have developed a structural model for turbulent wall bounded flows in which they solve the viscous flow equations for the inner flow and solve the outer flow using point vortex method. Dai et al. [134] have studied the flow over a backward facing step using Chorin's random vortex method. They found that the vortex method predicted the essential characteristics of internal recirculating turbulent flow. The calculated reattachment length agreed well with the experimental results. The equations of motion of point vortices represent a Hamiltonian system. The study of the dynamics of few vortex systems is expected to shed some light on the transition from laminar to turbulent flow and on the onset of chaos [126].

9.2 Large-Eddy Simulation

In large-eddy simulation, the filtered time dependent three-dimensional Navier-Stokes equation is integrated directly. Filtering is done to remove the small eddies and to obtain an equation for large eddies. It is essentially equal to averaging over a small spatial region or low-pass filtering the equations in Fourier-space. The effect of small eddies on the large ones has to be modeled. For a given flow, the dividing line between the small and large scale flow fields is determined by the computational grid resolution. When a large number of grid points is used, a large fraction of the turbulent eddies is directly calculated and only a small fraction has to be modeled. One important feature of LES is that most of the time-dependent characteristics of the flow are retained rather than lost in the averaging process.

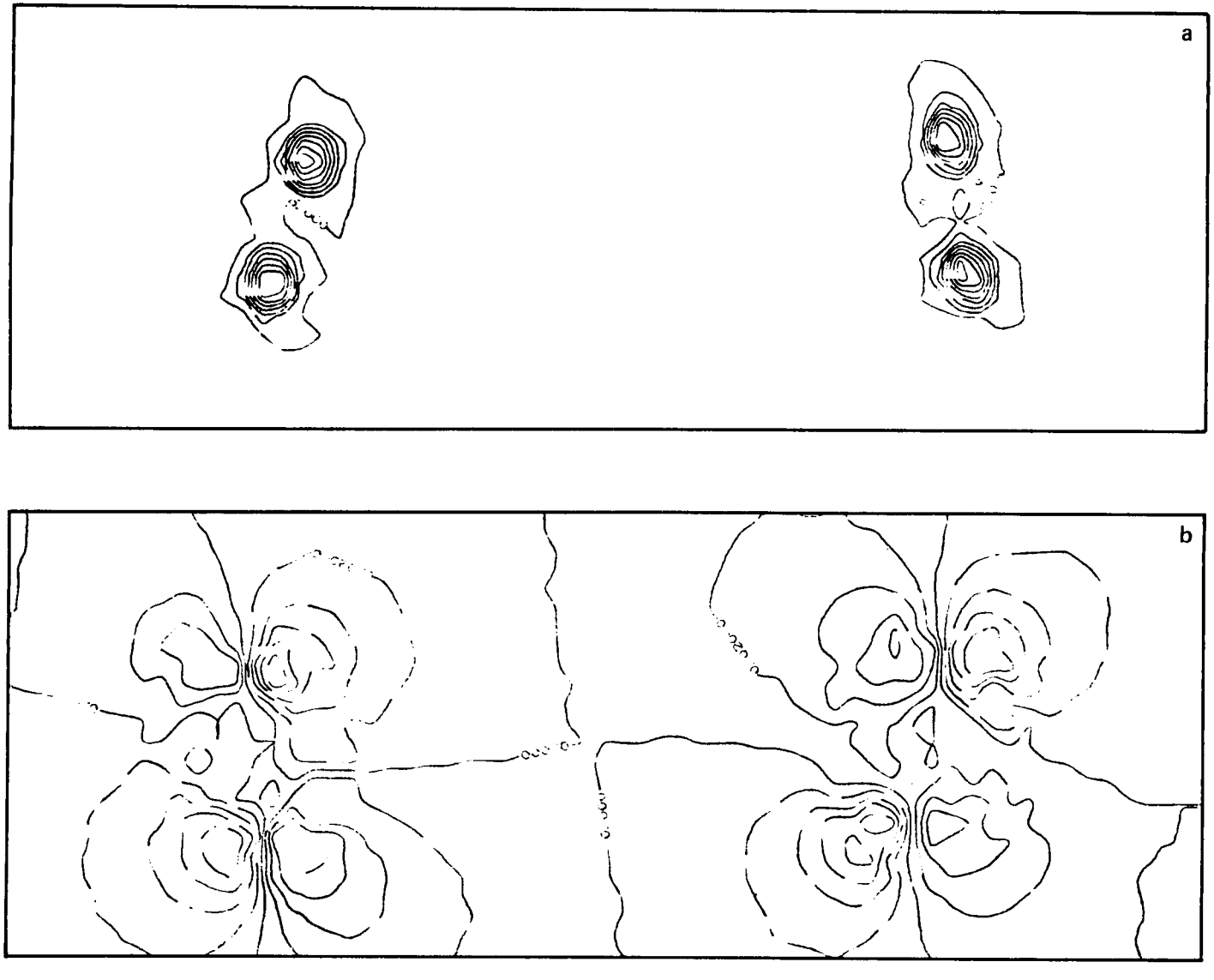

Figure 33. Contours of (a) vorticity and (b) coherent Reynolds stress during pairing in a mixing layer [129].

To obtain the equations for LES, Leonard [135] suggested the local spatial averaging:

$$\overline{u_i}(x) = \int G\,(x-x')\,u_i\,(x')\,dx' \tag{58}$$

where G is a normalized weighting function, which may be called a filter. Its effect is to remove the small scale fluctuations from u_i in forming $\overline{u_i}$, the large scale field, and u_i', the subgrid scale field. A simple choice is to let G = 1 within a cubic volume with sides of length Δ_a centered at x and let G = 0 outside. Then,

$$\overline{u_i}(x) = \frac{1}{\Delta_a{}^3}\iiint u_i\,(x_1-x_1',\, x_2-x_2',\, x_3-x_3')\,dx_1'\,dx_2'\,dx_3' \quad . \tag{59}$$

The integrations being from $x_1-1/2\ \Delta_a$ to $x_1 + 1/2\ \Delta_a$, $x_2 - 1/2\ \Delta_a$ to $x_2 + 1/2\ \Delta_a$ and $x_3 - 1/2\ \Delta_a$ to $x_3 + 1/2\ \Delta_a$.

The filtered counterparts of (1) and (2) can be obtained by multiplying (1) and (2) by the weighting function G = 1 and integrating over the cubic volume v

$$\frac{\partial \overline{u_i}}{\partial x_i} = 0 \tag{60}$$

$$\frac{\partial \overline{u_i}}{\partial t} + \frac{\partial}{\partial x_j}\,\overline{u_i u_j} = -\frac{\partial \overline{p}}{\partial x_i} + \nu\,\nabla^2\,\overline{u_i} \tag{61}$$

Now make the substitution $u_i = \overline{u_i} + u_i'$ in the nonlinear advective term to obtain

$$\frac{\partial \overline{u_i}}{\partial t} + \frac{\partial}{\partial x_j}\,\overline{\overline{u_i}\,\overline{u_j}} = -\frac{\partial \overline{p}}{\partial x_i} + \nu\,\nabla^2\,\overline{u_i} - \frac{\partial}{\partial x_j}\,\eta_{ij} \tag{62}$$

where

$$\eta_{ij} = \overline{\overline{u_i}\,\overline{u_j}}' + \overline{u_i'\,\overline{u_j}} + \overline{u_i'\,u_j'} \quad , \tag{63}$$

is the subgrid scale (SGS) Reynolds stress. Thus in LES one solves equations (60) and (62) together with (63). Since the small scale component of the velocity field u_i' is not computed, the terms containing it need to be modeled.

Deardorff [136] and Schumann [137] employ a different approach to obtain LES equations. The equations are set up for the grid employed based on integral conservation equations for each grid volume. The form of the equations are the same as (60) and (62) if the overbar is interpreted as the volume average. In this approach

$$\overline{\bar{u}_i \bar{u}_j} = \bar{u}_i \, \bar{u}_j \quad , \tag{64}$$

$$\overline{u_i'} = 0 \quad . \tag{65}$$

as in the time-averaging process. This reduces the SGS Reynolds stress to

$$\eta_{ij} = \overline{u_i' \, u_j'} \quad . \tag{66}$$

$\overline{u_i' u_j'}$ is modeled by eddy viscosity models.

The model often used is that due to Smagorinsky [138],

$$\overline{u_i' u_j'} = (C\Delta_a)^2 \left[\frac{1}{2} \left(\frac{\partial \bar{u}_i}{\partial x_j} + \frac{\partial \bar{u}_j}{\partial x_i} \right) \left(\frac{\partial \bar{u}_i}{\partial x_j} + \frac{\partial \bar{u}_j}{\partial x_i} \right) \right]^{1/2} \cdot \left(\frac{\partial \bar{u}_i}{\partial x_j} + \frac{\partial \bar{u}_j}{\partial x_i} \right) \tag{67}$$

where C is a constant which varies from 0.13 to 0.21. [When using the form (63), the term to be modeled is still only $\overline{u_i' u_j'}$ as the other terms can be taken care of by using equation (64) in equation (61) which results in a modified pressure gradient term [139]].

The near wall treatment is crucial as in the time averaged Reynolds stress modeling. For a successful LES simulation, one has to be able to resolve all the large eddies in the neighborhood of the wall and at a distance from the wall, since the near wall eddies are responsible for the turbulent energy production for the flow field. Moin and Kim [140] solve the LES equations up to the wall while Schumann [137] and Deardorff [136] carry out the calculations only to a point in the logarithmic layer where semi-empirical boundary conditions are used to near wall turbulence. In this approach the important near wall turbulence flow dynamics is modeled which limits the use of LES approach to the understanding of the flow physics.

The channel flow has been computed using the LES approach and found to reproduce experimental observations such as the turbulent bursting sequence, production of longitudinal vortices in boundary layers [138-140]. An example of the LES solution is shown in Figure 34. The figure shows contours of instantaneous velocity, pressure fluctuations and SGS kinetic energy in a channel flow. Clark et al. [141] evaluated the SGS Reynolds stress model constant and found that it agreed with the one obtained from theory and experiment. Though it is expected that the LES and direct simulations can help to improve the time averaged Reynolds stress modeling [139], no such improvement has ensued.

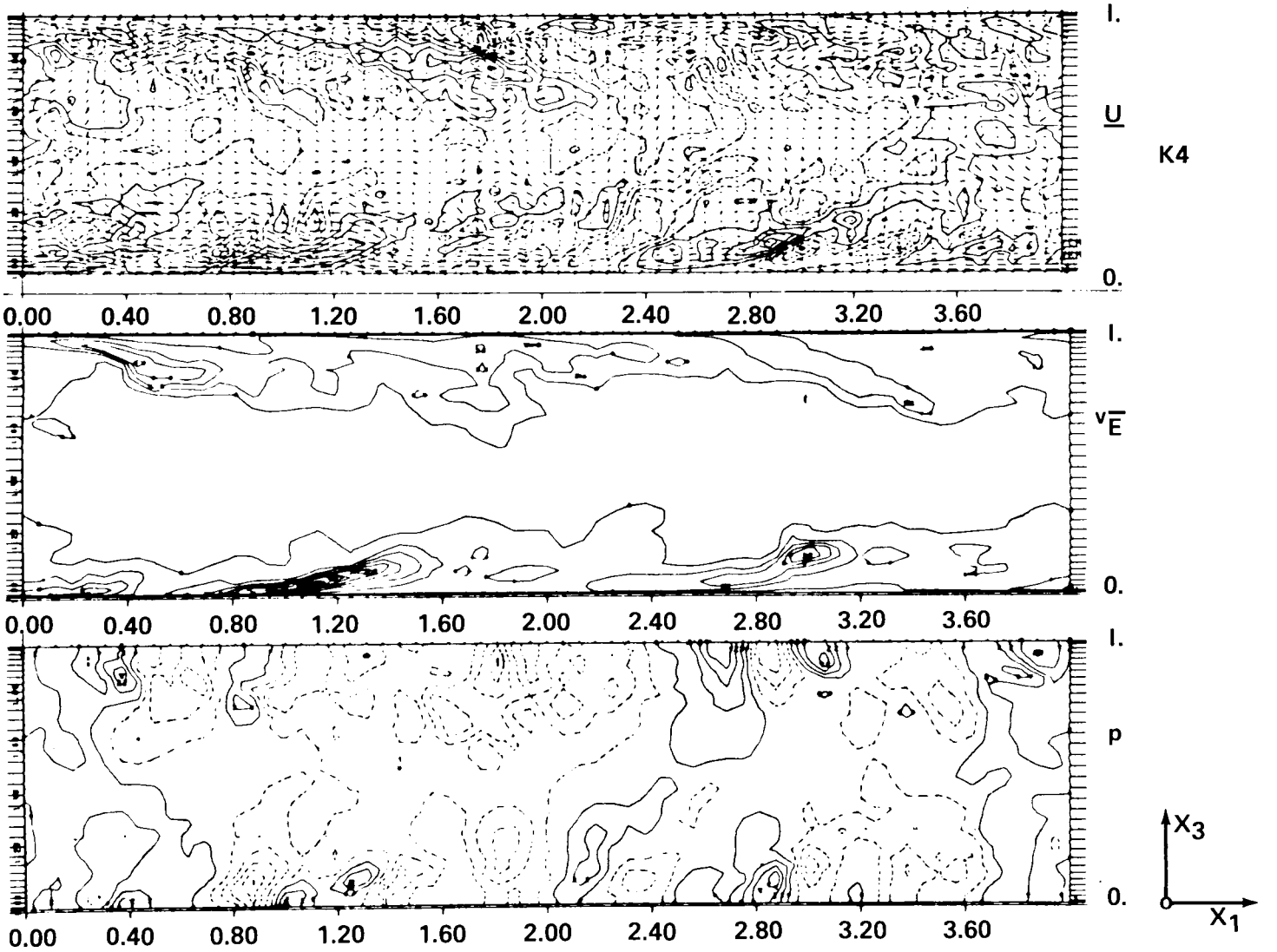

Figure 4. Contours of velocity, SGS kinetic energy and pressure fluctuations in a channel flow [137].

9.3 Direct or Full Simulation

In this approach one solves the time dependent three-dimensional Navier-Stokes equations for different scales of the flow (the smallest scale that can be resolved being determined by the number of grid points). This approach has been used mainly to homogeneous flows at low Reynolds numbers (of the order of R_t = 40), employing as much as 2 million grid points. Periodicity is assumed in all three dimensions. The velocity field is represented at every instant by a three-dimensional Fourier series in a coordinate system moving with the spatially linear mean flow [142]. In these coordinates the full Navier-Stokes equations admit spatially periodic solutions with fixed period for all time. The representation of statistical homogeneity in space by strict periodicity requires that the computational period be much longer than any turbulence scale containing significant energy. Also, the mesh size has to be much smaller than the turbulence dissipation scales. A low turbulence Reynolds number is required to limit the scales. With the present computer resources, only flows with a small range of energetic turbulence scales can be computed [142].

Large eddy simulation and direct simulation are not expected to become engineering calculation methods in the foreseeable future. However, these methods will help in the understanding of the physics of turbulent flows.

X. CONCLUSIONS

The report presents a brief account of various turbulence closure models and their applications to internal flows. A critical evaluation of the performance of the models is presented. The main conclusions are:

1. The k-ϵ model is the most widely used model for internal flows. It provides an efficient method of calculating engineering flows. The performance of the standard k-ϵ model becomes poor as we go from the attached flow, recirculating flow, swirl flow, to combusting flows in that order.

2. The standard k-ϵ model performs poorly in the prediction of apparently simple flow over a backward facing step. There is no significant improvement in the value of reattachment length predicted with modified near-wall models. Algebraic stress model should be used with modified ϵ-equation.

3. The k-ϵ model performance is rather poor for flows with streamline curvature. Algebraic stress model performs better for these flows.

4. Reynolds stress models have not been thoroughly tested for recirculating flows and swirl flows. Computational effort required for RSM is much greater than that required for the k-ϵ model.

5. For flows with regions of secondary flow (noncircular duct flows) algebraic stress model performs fairly well for fully developed flow. For developing flow RSM should be employed.

6. In many computations, the grid dependence of the solutions has not been achieved or tested due to the limitations of the computing resources. These solutions have to be taken with caution.

7. The initial conditions play a crucial role in the performance of the model and predicted solutions. Thus, use of appropriate initial conditions in the SSME flow computation is essential.

8. The TEACH (Teaching Elliptic Axisymmetric Characteristics Heuristically) code [143] or its variant is the most widely used computer code in the prediction of turbulent internal (plane 2D, axisymmetric, 3-D, swirl and reacting) flows, cited in the literature.

XI. RECOMMENDATIONS

Based on the present evaluation, the following suggestions for future work can be made:

1. More work is necessary to arrive at a better numerical scheme for the solution of the model equations.

2. A clear statement of the initial conditions employed should be mandatory for any presentation of the model predictions, especially when they are made "suitable" to match the experimental results.

3. The use of ASM models for flows with streamline curvature appears promising and needs further testing.

4. The use of the flux Richardson number for curved flows should be explored.

5. Detailed experimental data for curved flows with strong curvature are needed for the validation of the model predictions for these flows.

6. With the availability of more computing power, use of RSM models to account for curvature effects, countergradient transport and secondary flows would improve the confidence in turbulence closure models.

REFERENCES

1. Bradshaw, P., (Ed.): Turbulence. Springer-Verlag, 1978.

2. Tennekes, H. and Lumley, J. L.: A First Course in Turbulence. The MIT Press, 1972.

3. Hinze, J. O.: Turbulence. McGraw-Hill, 1975.

4. Reynolds, W. C.: Computation of Turbulent Flows. Ann. Rev. Fluid Mech., vol. 8, 1976, pp. 183-208.

5. Bradshaw, P., Ferris, D. H., and Atwell, N. P.: Calculation of Boundary-Layer Development Using the Turbulent Energy Equation. J. Fluid Mech., Vol. 28, 1967, pp. 593-616.

6. Cebeci, T., Chang, K. C., and Bradshaw, P.: Solution of Hyperbolic System of Turbulence-Model Equations by the "Box" Scheme. Comput. Methods in Appl. Mech. Engr., Vol. 22, 1980, pp. 213-227.

7. Mellor, G. L. and Herring, H. J.: A Survey of the Mean Turbulent Field Closure Models. AIAA J., Vol. 11, 1973, pp. 590-599.

8. Bradshaw, P.: The Understanding and Prediction of Turbulent Flow. Aero. J., Vol. 76, 1972, pp. 403-417.

9. Launder, B. E. and Spalding, D. B.: Mathematical Models of Turbulence. Academic Press, London, 1972.

10. Bradshaw, P. and Cebeci, T.: Engineering Calculation Methods. Academic Press, London, 1978.

11. Gosman, A. D., Pun, W. M., Runchal, A. K., Spalding, D. B., and Wolfshtein, M.: Heat and Mass Transfer in Recirculating Flows. Academic Press, London, 1969.

12. Launder, B. E. and Spalding, D. B.: Turbulence Models and Their Applications to the Prediction of Internal Flows. Heat and Fluid Flow, Vol. 2, 1972, pp. 43-54.

13. Rotta, J. C.: Prediction Methods for Turbulent Flows. Von Karman Institute for Fluid Dynamics, Lecture Series 76, 1975.

14. Lumley, J. L.: Computational Modeling of Turbulent Flows. Advances in Appl. Mech., Vol. 18, 1978, pp. 123-176.

15. Rodi, W.: Examples of Turbulence Models for Incompressible Flows. AIAA J., Vol. 20, 1982, pp. 872-879.

16. Spalding, D. B.: Turbulence Models, a Lecture Course. Imperial College of Science and Technology, 1982.

17. Lumley, J. L.: Turbulence Modeling. J. App. Mech., 50th Anniversary Issue, 1983, pp. 1097-1103.

18. Marvin, J. G.: Turbulence Modeling for Computational Aerodynamics. AIAA J., Vol. 21, 1983, pp. 941-955.

19. Murphy, J. D.: Turbulence Modeling. NASA TM 85889, 1984.

20. Donaldson, C. duP.: Calculation of Turbulent Shear Flows for Atmospheric and Vortex Motions. AIAA J., Vol. 10, 1972, pp. 4-12.

21. Launder, B. E. and Spalding, D. B.: The Numerical Computation of Turbulent Flows. Compu. Methods in Appl. Mech. Engr., Vol. 3, 1974, pp. 269-289.

22. Schetz, J. A.: Injection and Mixing in Turbulent Flow. (Progress in Astronautics and Aeronautics, Vol. 68), AIAA, New York, 1980.

23. Launder, B. E., Reece, G. J., and Rodi. W.: Progress in the Development of a Reynolds Stress Turbulence Closure. J. Fluid Mech., Vol. 68, 1975, pp. 537-586.

24. Schumann, U.: Realizability of Reynolds Stress Turbulence Models. Phys. Fluids, Vol. 20, 1977, pp. 721-725.

25. Rodi, W.: A New Algebraic Relation for Calculating the Reynolds Stresses. ZAMM, Vol. 56, 1976, pp. T219-T221.

26. Hanjalic, H., Launder, B. E., and Schistel, R.: Multiple-Time-Scale Concepts in Turbulent Transport Modeling. Proc. Turbulent Shear Flows, 2, 1979, pp. 10.31-10.36.

27. Jones, W. P. and Launder, B. E.: The Prediction of Laminarization with a Two-Equation Model of Turbulence. Int. J. Heat Mass Transfer, Vol. 5, 1973, pp. 301-314.

28. Chieng, C. C. and Launder, B. E.: On the Calculation of Turbulent Transport Downstream from an Abrupt Pipe Expansion. Num. Heat Transfer, Vol. 3, 1980, pp. 189-207.

29. Amano, R. S.: Development of a Turbulence Near-Wall Model and Its Application to Separated and Reattached Flows. Numerical Heat Transfer, Vol. 7, 1984, pp. 59-75.

30. Iacovides, H. and Launder, B. E.: PSL – An Economical Approach to the Numerical Analysis of Near-Wall, Elliptic Flow. J. Fluids Engineering, Vol. 106, 1984, pp. 241-242.

31. Launder, B. E.: Numerical Computation of Convective Heat Transfer in Complex Turbulent Flows: Time to Abandon Wall Functions? Int. J. Heat Mass Transfer, Vol. 27, 1984, pp. 1485-1491.

32. Bradshaw, P.: Effects of Streamline Curvature on Turbulent Flows. AGARDograph, No. 169, 1973.

33. Gibson, M. M.: An Algebraic Stress and Heat Flux Model for Turbulent Shear Flow with Streamline Curvature. Int. J. Heat Mass Transfer, Vol. 21, 1978, pp. 1609-1617.

34. Pourahmadi, F. and Humphrey, J. A. C.: Prediction of Curved Channel Flow with an Extended k-ϵ Model of Turbulence, Vol. 21, 1983, pp. 1365-1373.

35. Launder, B. E., Priddin, C. H., and Sharma, B. I.: The Calculation of Turbulent Boundary Layers on Spinning and Curved Surfaces. J. Fluids Engineering, 1977, p. 231-239.

36. Militzer, J., Nicoll, W. B., and Alpay, J. A.: Some Observations on the Numerical Calculation of the Recirculating Region of Twin Parallel Symmetric Jet flow. Proc. Symp. on Turbulent Shear Flows. Pennsylvania State University, 1977, pp. 18.11-18.18.

37. Leschziner, M. A. and Rodi, W.: Calculation of Annular and Twin Parallel Jets Using Various Discretization Schemes and Turbulence Model Variations. J. Fluids Engr., Vol. 103, 1981, pp. 352-360.

38. So, R. M. C.: Discussion on Reference 37 and Author's Closure. J. Fluids Engr., Vol. 103, 1981, pp. 263-265.

39. Lilley, D. G.: Prediction of Inert Turbulent Swirl Flows. AIAA J., Vol. 1, 11, 1973, pp. 955-960.

40. So, R. M. C.: Turbulence Velocity Scales for Swirling Flows, Turbulence in Internal Flows, Project Squid Workshop, Hemisphere Publishing Corp., Washington, D.C., 1977.

41. Srinivasan, R., and Mongia, H. C.: Numerical Computation of Swirling Recirculating Flows. Final Report, NASA CR-165196, 1980.

42. Rodi, W.: Influence of Buoyancy and Rotation on Equations for the Turbulent Length Scale. Proc. 2nd Symp. on Turbulent Shear Flows. London, Imperial College, 1979, pp. 10.37-10.42.

43. Kline, S. J., Cantwell, B. J., and Lilley, G. M. (Ed.): The 1980-1981 AFOSR-HTTM-Stanford Conference on Complex Turbulent Flows, Stanford University, I, II, and III.

44. Mansour, N. N. and Morel, T.: ibid III, pp. 1418-1423.

45. Pollard, A.: ibid III, pp. 1486-1490.

46. Rodi, W., et al.: ibid III, pp. 1495-1516.

47. Launder, B. E., et al.: ibid III, pp. 1390-1407.

48. Spalding, D. B.: et al.: ibid III, pp. 1521-1526.

49. Demirdzic, I., Gosman, A. D., and Issa, R. I.: ibid III, pp. 1383-1389.

50. Donaldson, C. duP., et al.: ibid III, pp. 1342-1345.

51. Ilegbusi, J. O. and Spalding, D. B.: Turbulent Flow Downstream of a Backward Facing Step. Proc. 4th Int. Symposium on Turbulent Shear Flows, Karlsruhe, 1983.

52. Nallsamy, M.: Computation of Recirculating Flows Using PHOENICS code. In progress 1985.

53. Syed, S. and Chiappetta, L.: Finite Difference Methods for Reducing Numerical Diffusion in Teach-Type Calculations. AIAA Paper, AIAA-85-0056, 1985.

54. Kim. J., Kline, S., and Johnston, J.: Investigation of Separation and Reattachment of a Turbulent Shear Layer, Flow Over a Backward Facing Step. Report MD.37, Mech. Eng. Stanford University.

55. Tropea, C. and Durst, F.: Evaluators Comment. 1981 AFOSR-HTTM-Stanford Conference on Complex Turbulent Flows, 1981.

56. Launder, B. E.: 1981-Stanford Conference on Complex Turbulent Flows: Computation and Experiment, Vol. II, pp. 843-862.

57. Pope, S. B.: An Explanation of the Turbulent Round Jet/Plane Jet Anomaly. AIAA J., Vol. 16, 1978, pp. 279-281.

58. Wood, P. E. and Chen, C. P.: Turbulence Model Predictions of the Radial Jet – A Comparison of k-ϵ Models. Can. J. Ch. E., in press, 1985.

59. Gosman, A. D., Khalil, E. E., and Whitelaw, J. H.: The calculation of Two-Dimensional Turbulent Recirculating Flows. Turbulent Shear Flows, Vol. 2, 1980, pp. 237-255.

60. Abbott, D. E. and Kline, S. J.: Experimental Investigation of Subsonic Turbulent Flow Over Single and Double Backward Facing Steps. J. Basic Eng., Vol. 84, 1962, pp. 317-325.

61. Durst, F. and Rastogi. A. K.: Theoretical and Experimental Investigations of Turbulent Flows with Separation. Turbulent Shear Flow, Vol. 2, 1980, pp. 208-219.

62. Qin, H.: The Flow Characteristic of a Sudden Axisymmetric Expansion. PDR/CPDU IC/4, Imperial College of Science and Technology, London, 1984.

63. Ha Minh, H. and Chassaing, P.: Perturbation of Turbulent Pipe Flow. Turbulent Shear Flow, Vol. 3, 1981, pp. 178-197.

64. Moon, L. F. and Rudinger, G.: Velocity Distribution in an Abruptly Expanding Circular Duct. J. Fluids Engineering, 1977, pp. 226-230.

65. Chen, C. P.: Flow in a Pipe Expansion. Effect of Inlet Swirls, to be published.

66. Amano, R. S.: A Study of Turbulent Flow Downstream of an Abrupt Pipe Expansion. AIAA J., Vol. 21, 1983, pp. 1400-1405.

67. Amano, R. S. and Goel, P.: A Numerical Study of a Separating and Reattaching Flow by Using Reynolds Stress Turbulence Closure. Num. Heat Transfer, Vol. 7, 1984, pp. 343-357.

68. Back, L. H. and Roschke, E. J.: Shear Layer Flow Regimes and Wall Instabilities and Reattachment Lengths Downstream of an Abrupt Circular Channel Expansion. J. Appl. Mech., Vol. 94, 1972, pp. 677-681.

69. Chaturvedi, M. C.: Flow Characteristics of an Axisymmetric Expansion. J. Hyd. Div., Proc. ASCE, Vol. 89, 1963, pp. 61-92.

70. Pope, S. B. and Whitelaw, J. H.: The Calculation of Near Wake Flows. J. Fluid Mech., Vol. 73, 1976, pp. 9-32.

71. Habib, M. A. and Whitelaw, J. H.: Velocity Characteristics of a Confined Coaxial Jet. J. Fluids Engineering, Vol. 101, 1979, pp. 521-529.

72. Habib, M. A. and Whitelaw, J. H.: Velocity Characteristics of Confined Coaxial Jets With and Without Swirl. J. Fluid Engineering, Vol. 102, 1980, pp. 47-53.

73. Habib, M. A. and Whitelaw, J. H.: The Calculation of Turbulent Flow in Wide-Angle Diffusers. Num. Heat Transfer, Vol. 5, 1982, pp. 145-164.

74. Rhode, D. L., Lilley, D. G., and McLaughlin, D. K.: On The Prediction of Swirling Flow Fields Found in Axisymmetric Combustor Geometries. J. Fluids Engineering, Vol. 104, 1982, pp. 378-392.

75. Honami, S., Ariga, I., Abe, T., and Watonabe, I.: Investigation of Turbulent Flows in Curved Channel Flows. ASME Paper 75-FE-32, 1975.

76. Ellis, L. B. and Joubert, P. N.: Turbulent Shear Flow in a Curved Duct. J. Fluid Mech., Vol. 62, 1974, pp. 65-84.

77. Towne, C. E.: Computation of Viscous Flow in Curved Ducts and Comparison with Experimental Data. AIAA Paper No. AIAA-84-0531, 1984.

78. Mukerjee, T., Singhal, A. K., Tam, L. T., Costes, N. C., and Fichtl, G. H.: Analysis of Turbulent Flow and Heat Transfer in SSME Turnaround Ducts, to be submitted, 1985.

79. Owens, S. F., Mukerjee, T., Przekwas, A. J., Singhal, A. K., and Costes, N. C.: Analysis of Turbulent, Compressible Flow in Hot Gas Manifold (Phase 2 – Design) of Space Shuttle Main Engine. To be submitted to J. of Spacecraft and Rockets, 1985.

80. Agarwal, Y., Talbot, L., and Grong, K.: Laser Anemometer Study of Flow Development in Curved Circular Pipes. J. Fluid Mech., Vol. 85, 1978, pp. 497-518.

81. Nuttal, J. B., Axial Flow in a Vortex. Nature, Vol. 172, 1953, pp. 582-583.

82. Gupta, A. K., Lilley, D. G., Syred, N.: Swirl Flows. ABACUS Press, 1984.

83. Jones, W. P. and Whitelaw, J. H.: Calculation Method for Reacting Turbulent Flows: A Review. Combustion and Flame, Vol. 48, 1982, pp. 1-26.

84. Novick, A. S., Miles, G. A., and Lilley, D. G.: Numerical Simulation of Combustor Flow Fields: A Primitive Variable Design Capability. J. Energy, Vol. 3, 1979, pp. 95-105.

85. Novick, A. S., Miles, G. A., and Lilley, D. G.: Modeling Parameter Influences in Gas Turbine Combustor Design. J. Energy, Vol. 3, 1979, pp. 257-262.

86. Ramos, J. I.: Turbulent Nonreacting Swirling Flows. AIAA J., Vol. 22, 1983, pp. 846-848.

87. Sturgess, G. J., Syed, S. A., and McManus, K. R.: Importance of Inlet Boundary Conditions for Numerical Simulation of Combustor Flows. AIAA Paper, No. AIAA-83-1263.

88. Boysan, F. and Swithenbank, J.: Discussion on the Paper by Rhode et al. [64]. J. Fluids Engineering, Vol. 104, 1982, pp. 391-392.

89. Escudier, M. P., Bronstein, J., and Zehnder, N.: Observations and LDA measurements of Confined Vortex Flow. J. Fluid Mech., Vol. 98, 1980, pp. 49-63.

90. Dixon, T. F., Truelove, J. S., and Wall, T. F.: Aerodynamic Studies on Swirled Coaxial Jets from Nozzles with Divergent Quarls. J. Fluids Engineering, Vol. 105, 1983, pp. 197-203.

91. Boysan, F., Ayers, W. H., and Swithenbank, J.: A Fundamental Mathematical Modeling Approach to Cyclone Design. Trans. I. Chem. E., Vol. 60, 1982, pp. 223-230.

92. Speziale, C. G.: On Turbulent Secondary Flows in Pipes of Noncircular Cross-Section. Int. J. Engr. Sci., Vol. 20, 1982, pp. 861-872.

93. Launder, B. E. and Ying, W. M.: Prediction of Flow and Heat Transfer in Ducts of Square Cross Section. Heat and Fluid Flow, Vol. 3, 1973, pp. 115-121.

94. Hanjalic, K. and Launder, B. E.: A Reynolds Stress Model of Turbulence and Its Application to Thin Shear Flows. J. Fluid Mech., Vol. 52, 1972, pp. 609-638.

95. Gosman, A. D. and Rapley, C. N.: The Analysis of Fully Developed Turbulent Flow Through Non-Circular Passages. Paper No. FS178, Proc. of Int. Conf. on Numerical Methods, 1978.

96. Launder, B. E. and Ying, W. M.: Secondary Flows in Ducts of Square Cross Section. J. Fluid Mech., Vol. 54, 1972, pp. 289-295.

97. Reece, G. A.: A Generalized Reynolds Stress Model of Turbulence. Ph.D. Thesis, University of London, 1976.

98. Noat, D., Shavit, A., and Wolfshtein, M.: Numerical Calculation of Reynolds Stresses in a Square Duct with Secondary Flow. Warme-und-Stoffubentragnug, Vol. 7, 1974, pp. 151-161.

99. Brundrett, E. and Baines, W. D.: The Production and Diffusion of Vorticity in Duct Flows. J. Fluid Mech., Vol. 19, 1964, pp. 375-394.

100. Nakayama, A., Chow, W. L., and Sharma, D.: In the 1980-81 AFOSR-HTTM Stanford Conference on Complex Turbulent Flows, Vol. III, pp. 1312-1317.

101. Coustiex, J., et al.: In the 1980-81 AFOSR-HTTM Stanford Conference on Complex Turbulence Flows, Vol. III, pp. 1326-1336.

102. de Vahl Davis, G. and Mallinson, G. D.: An Evaluation of Upwind and Central Difference Approximations by a Study of Recirculating Flow. Computers and Fluids, 1976, pp. 29-37.

103. Raithby, G. D.: A Critical Evaluation of Upstream Differencing Applied to Problems Involving Fluid Flow. Comp. Meths. Appl. Mech. Eng., Vol. 9, 1976, pp. 75-103.

104. McGuirk, J. J., Taylor, A. M. K. P., and Whitelaw, J. H.: The Assessment of Numerical Diffusion in Upwind Difference Calculations. Turbulent Shear Flow 2, 1980, pp. 206-224.

105. Raithby, G. D.: Skew Upwind Differencing Schemes for Problems Involving Fluid Flow. Comp. Meths. Appl. Mech. Eng., Vol. 9, 1976, pp. 153-165.

106. Leschziner, M. A.: Practical Evaluation of Three Finite Difference Schemes for the Computation of Steady State Recirculating Flows. Comp. Meth. Appl. Mech. Eng., Vol. 23, 1980, pp. 293-312.

107. Leschziner, M. A. and Rodi, W.: Computation of Strongly Swirling Axisymmetric Free Jets. AIAA J., Vol. 22, 1984, pp. 1742-1747.

108. Syed, S. A. and Sturgess, G. J.: In Momentum and Heat Transfer Processes in Recirculating Flows. ASME HTD 13, 1980, p. 71.

109. Roback, R. and Johnson, B. V.: Mass and Momentum Turbulent Transport Experiments with Confined Swirling Coaxial Jets. NASA CR-168252, 1983.

110. Johnson, B. V. and Bennett, J. C.: Mass and Momentum Turbulent Transport Experiments with Confined Coaxial Jets. NASA CR-165574, 1981.

111. Beguier, C., Giralt, F., Fulachier, L., and Keffer, J. F.: Negative Production in Turbulent Shear Flows. In. Lecture Notes in Physics, Vol. 76, 1978, pp. 22-35.

112. Townsend, A. A.: The Structure of Turbulent Shear Flows. Cambridge University Press, 1976.

113. Hinze, J. O.: Turbulent Flow Regions with Shear Stress and Mean Velocity Gradient of Opposite Sign. J. App. Sci. Res., Vol. 22, 1970, pp. 163-175.

114. Brown, G. L. and Roshko, A.: On Density Effects and Large Structure in Turbulent Mixing Layers. J. Fluid Mech., Vol. 64, 1974, pp. 775-816.

115. Winant, C. D. and Browand, F. K.: Vortex Pairing: A Mechanism of Turbulent Mixing Layer Growth at Moderate Reynolds Number. J. Fluid Mech., Vol. 63, 1974, pp. 237-255.

116. Nallasamy, J. and Hussain, A. K. M. F.: Response of the Axisymmetric Mixing Layer to Sub-harmonic Forcing at Different Amplitudes. Proc. 8th Biennial Turbulence Symposium, Rolla, 1983.

117. Oster, D. and Wygnanski, I.: The Forced Mixing Layer Between Parallel Streams. J. Fluid Mech., Vol. 123, 1982, pp. 91-130.

118. Libby, P. A. and Bray, K. N. C.: Implications of Laminar Flamlet Model in Pre-Mixed Turbulent Combustion. Combustion and Flame, Vol. 39, 1980, pp. 33-41.

119. Libby, P. A. and Bray, K. N. C.: Countergradient Diffusion in Premixed Turbulent Flames. AIAA J., Vol. 19, 1981, pp. 205-213.

120. Favre, A.: Equations des gas Turbulents Compressibles. J. Mechanique, Vol. 4, 1965, p. 361.

121. Spalding, D. B.: The Two-Fluid Model of Turbulence Applied to Combustion Phenomena. AIAA Paper No. AIAA-84-0476, 1984.

122. Spalding, D. B.: A General Purpose Computer Programme for Multi-Dimensional One and Two Phase Flow, Mathematics and Computers in Simulation. North Holland Press, Vol. XXIII, 1981, pp. 267-276.

123. Patankar, S. V.: Numerical Heat Transfer and Fluid Flow. Hemisphere, 1980.

124. Saffman, P. G. and Baker, G. R.: Vortex Interactions. Ann. Rev. Fluid Mech., Vol. 11, 1976, pp. 95-122.

125. Leonard, A.: Vortex Methods for Flow Simulation. J. Comp. Physics, Vol. 37, 1980, pp. 289-335.

126. Aref, H.: Integrable, Chaotic, and Turbulent Vortex Motion in Two-Dimensional Fluid Flows. Ann. Rev. Fluid Mech., Vol. 15, 1983, pp. 345-389.

127. Acton, E.: A Modelling of Large Eddies in an Axisymmetric Jet. J. Fluid Mech., Vol. 98, 1980, pp. 1-31.

128. Nallasamy, M. and Hussain, A. K. M. F.: Numerical Study of the Phenomenon of Turbulence Suppression in a Plane Shear Layer. Turbulent Shear Flows, Vol. 4, 1984, pp. 169-181.

129. Nallasamy, M. and Hussain, A. K. M. F.: Numerical Simulation of "Flapping" and "Puffing" Instabilities in a Plane Jet. To be published.

130. Chorin, A. J.: Numerical Study of Slightly Viscous Flow. J. Fluid Mech., Vol. 57, 1973, pp. 785-796.

131. Chorin, A. J.: Flame Advection and Propagation Algorithms. J. Comput. Phys., Vol. 35, 1980, p. 1-11. See also: The Evolution of a Turbulent Vortex, Commun. Math. Phys., Vol. 83, 1982, pp. 526-527.

132. Ghoniem, A. F., Chorin, A. J., and Oppenheim, A. K.: Numerical Modeling of Turbulent Flow in a Combustion Tunnel. Phil. Trans. Roy. Soc. London, Ser. A, Vol. 304, 1982, pp. 303-325.

133. Beljaars, A. C. M., Krishna Prasad, K., and de Vries, D. A.: A Structural Model for Turbulent Exchange in Boundary Layers. Vol 112, 1981, pp. 33-70.

134. Dai, Y. W., Ghoniem, A. F., Sherman, F. S., and Oppenheim, A. K.: Numerical Modeling of Turbulent Flow in a Channel. NASA CR-168278, 1983.

135. Leonard, A.: Energy Cascade in Large Eddy Simulations of Turbulent Fluid Flows. Adv. in Geophys., Vol. 18A, 1973, pp. 237-247.

136. Deardorff, J. W.: A Numerical Study of Three-Dimensional Turbulent Flow at Large Reynolds Numbers. J. Fluid Mech., Vol. 41, 1970, pp. 453-480.

137. Schumann, U.: Subgrid Scale Model for Finite Difference Simulations of Turbulent Flows in Plane Channels and Annuli. J. Comp. Physics, Vol. 18, 1975, pp. 376-404.

138. Smagorinsky, J.: General Circulation Experiments with Primitive Equations: I. The Basic Experiment. Mon. Weath. Rev., Vol. 91, 1963, pp. 99-164.

139. Ferzieger, J. H.: Higher Level Simulation of Turbulent Flows. In "Computational Methods for Turbulent, Transonic and Viscous Flows." Ed. J. A. Eassers, Hemisphere/Springer, 1983, pp. 93-182.

140. Moin, P. and Kim, J.: Numerical Investigation of Turbulent Channel Flows. J. Fluid Mech., Vol. 118, 1981, pp. 341-377.

141. Clark, R. A., Ferzieger, J. H., and Reynolds, W. C.: Evaluation of Subgrid-Scale Models Using an Accurately Simulated Turbulent Flow. J. Fluid Mech., Vol. 91, 1970, pp. 1-16.

142. Rogallo, R. S.: Numerical Experiments in Homogeneous Turbulence. NASA TM-81315, 1981.

143. Gosman, A. D. and Pun, W. M.: Calculation of Recirculating Flows. Rept. No. HTS/74/12, 1974, Dept. of Mechanical Engineering, Imperial College, London, England.

TECHNICAL REPORT STANDARD TITLE PAGE

1. REPORT NO.	2. GOVERNMENT ACCESSION NO.	3. RECIPIENT'S CATALOG NO.
NASA TP- 2474		

4. TITLE AND SUBTITLE	5. REPORT DATE
A Critical Evaluation of Various Turbulence Models as Applied to Internal Fluid Flows	May 1985
	6. PERFORMING ORGANIZATION CODE
7. AUTHOR(S) M. Nallasamy	8. PERFORMING ORGANIZATION REPORT #
9. PERFORMING ORGANIZATION NAME AND ADDRESS George C. Marshall Space Flight Center Marshall Space Flight Center, Alabama 35812	10. WORK UNIT NO. M-486
	11. CONTRACT OR GRANT NO.
	13. TYPE OF REPORT & PERIOD COVERED Technical Paper
12. SPONSORING AGENCY NAME AND ADDRESS National Aeronautics and Space Administration Washington, D.C. 20546	14. SPONSORING AGENCY CODE

15. SUPPLEMENTARY NOTES

Prepared by Systems Dynamics Laboratory, Science and Engineering Directorate.

16. ABSTRACT

The report presents a brief account of various turbulent models employed in the computation of turbulent flows, and evaluates the application of these models to internal flows by examining the predictions of various turbulence models in selected important flow configurations. The main conclusions of this analysis are: (a) The k-ϵ model is used in a majority of all the two-dimensional flow calculations reported in the literature. (b) Modified forms of the k-ϵ model improve the performance for flows with streamline curvature and heat transfer. (c) For flows with swirl, the k-ϵ model performs rather poorly; the algebraic stress model performs better in this case. (d) For flows with regions of secondary flow (noncircular duct flows), the algebraic stress model performs fairly well for fully developed flow. For developing flow, the algebraic stress model performance is not good; a Reynolds stress model should be used.

Two important factors in the numerical solution of the model equations, namely false diffusion and inlet boundary conditions, are discussed. The existence of countergradient transport and its implications in turbulence modeling are mentioned. Two examples of recirculating flow predictions obtained using PHOENICS code are discussed. Other approaches to turbulent flow computations, such as the vortex method, large eddy simulation (modeling of subgrid scale Reynolds stresses), and direct simulation, are briefly discussed. Finally, some recommendations for improving the model performance are made. The need for detailed experimental data in flows with strong curvature is emphasized.

17. KEY WORDS	18. DISTRIBUTION STATEMENT
Turbulent Flow Internal Flow Turbulence Models Computational Fluid Dynamics	Unclassified - Unlimited Subject Category 34

19. SECURITY CLASSIF. (of this report)	20. SECURITY CLASSIF. (of this page)	21. NO. OF PAGES	22. PRICE
Unclassified	Unclassified	70	A04

For sale by National Technical Information Service, Springfield, Virginia 22161

NASA-Langley, 1985

National Aeronautics and
Space Administration

Washington, D.C.
20546

Official Business
Penalty for Private Use, $300

THIRD-CLASS BULK RATE

Postage and Fees Paid
National Aeronautics and
Space Administration
NASA-451

NASA

POSTMASTER: If Undeliverable (Section 158 Postal Manual) Do Not Return